TFA

ACTA FACULTATIS TECHNICAE

TECHNICAL UNIVERSITY IN ZVOLEN

1

ISSUE: XXIX ZVOLEN 2024

Medzinárodný zbor recenzentov / International Reviewers Board

TABLE OF CONTENTS

SCIENTIFIC PAPERS

SCIENTIFIC PAPERS

EVALUATION OF FORAGE HARVESTING TECHNIQUES

HODNOCENÍ TECHNOLOGICKÝCH LINEK NA SKLIZEŇ PÍCE

Libor Matyáš[1], Michal Strnad[1], František Horejš[1], Martin Císler[1], František Tošovský[1]

[1]Czech University of Life Sciences Prague, Department of Agricultural Machines, Faculty of Engineering, Kamycka 129, 165 21 Prague 6 – Suchdol, Czech Republic, matyasl@tf.czu.cz, strnadmichal@tf.czu.cz, horejsf@tf.czu.cz, cisler@tf.czu.cz, tosovsky@tf.czu.cz

ABSTRACT: This paper presents the results of a field experiment evaulated using different mowing machines to the drying rate of forage, second cut grass. Disc mower with conditioner and drum mower both with rotary blades. Furthermore, the influence of the number of tedding on the forage drying process was evaluated. The field experiment took place in the north-eastern part of the Czech Republic during the 2022 season in August. The test field was divided into four parts (A, B, C, D). The first two parts (A, B) were cut with a drum mower without conditioner. The third and fourth parts (C, D) were mowed with a disc mower with conditioner. The tedding of forage took place on all parts during day 3 and day 5. On day 4, only parts B and D were tedded. During the experiment, samples were taken sequentially after a given activity (mowing, tedding) to compare the dry matter content of each section. The evaluation of dry matter content was obtained from the dried residual weight of the forage sample. The forage samples taken for the first two measurements did not show statistically significant differences in dry matter content. Due to several rainfall events, no significant loss of moisture content of forage was observed between the first two measurements. Significant loss of moisture content was observed between measurements 2 and 3. The forage that was conditioned and more times tedded showed on average higher moisture loss.

Keywords: forage, moisture loss, conditioning

ABSTRAKT: Tato práce představuje výsledky polního experimentu, při kterém byly porovnávány dva žací rotační stroje a jejich vliv na průběh sušení píce při druhé sklizni píce. Porovnáván byl diskový žací stroj s čechračem a bubnový žací stroj bez výbavy pro úpravu píce. Dále byla zjišťován vliv počtu obracení píce na průběh sušení píce. Pokusný pozemek se nachází v obci Orlické Záhoří, v severovýchodní části České republiky. Experiment byl uskutečněn během sklizňové sezóny v srpnu roku 2022. Pokusný pozemek byl rozdělen do čtyř částí (A, B, C, D). Nejprve proběhlo sečení prvních dvou částí (A, B) pozemku pomocí bubnového žacího stroje. Následovalo sečení druhých dvou částí (C, D) diskovým žacím strojem vybaveným čechracím rotorem. Třetí den proběhlo rozhození řádků na široko všech částí (A. B, C, D). Čtvrtý den proběhlo obrácení pouze části B a D. Pátý den proběhlo obrácení všech čtyř částí (A, B, C, D). Během experimentu byly po každém úkonu (sečení, obracení) odebrány vzorky z jednotlivých částí pozemku. Vzorky byly uloženy do neprodyšných sáčků pro následné dosušení a určení obsahu sušiny. Odebrané vzorky píce pro prv-

ní dvě měření nevykazovaly statisticky významné rozdíly v podílu sušiny. Vzhledem k několika dešťovým srážkám nebyl zaznamenán mezi prvními dvěma měřeními ani výrazný úbytek vlhkosti píce. Výraznější úbytek vlhkosti byl zaznamenán mezi měřením č. 2 a 3. U vzorků odebraných pro měření č. 3 zaznamenán statisticky významný rozdíl v podílu sušiny. Píce, která byla čechrána a vícekrát obrácena, vykazovala průměrně vyšší hodnoty podílu sušiny, avšak na hranici statistické významnosti.

Kľúčové slová: píce, úbytek vlhkosti, čechrání

INTRODUCTION

Forage crops are very important plant-based feed. It is an indispensable roughage that plays a decisive role in the production and quality of meat, milk and other animal products. The quality of harvested forage has a significant impact not only on animal health but also on yield. A common method for preserving forage is through drying. The cut forage is spread out over a plot, tedded multiple times, and then removed from the plot once it reaches the desired moisture level. It can then be stored freely or in square or round bales. The duration of time that forage is available on the land is a crucial factor and can be impacted by abrupt weather changes. Forage exposed to rain for extended periods loses nutritional value, so we aim to minimize exposure time. A commonly used method in recent decades is to condition freshly cut fodder. Disturbing stems and other parts of the plant can increase the rate of water evaporation from forage. When harvesting forage in the form of haylage, this is often the only step between mowing and harvesting (Mašek *et al.* 2011).

In case of adding low quality conservated forage to the feed ration, the need for grain feed increases. Some of the forage crops can be harvested up to five times under favourable conditions. An important factor is climatic conditions, which may be varied from region to region. In mountainous areas the growing season is shorter and therefore the harvesting period is shorter (Cempírková *et al.* 2008).

When planning forage harvesting, it is important to consider not only the weather but also the maturity stage of the crops to be harvested. Delaying the harvest date may lead to a reduction in available energy of 0.26 MJ/kg dry matter for grasses and up to 0.78 MJ/kg dry matter for clovers. In this case, the losses are qualitative. Quantitative losses may occur due to failure to mow or loss of nutritionally important parts when forage is tedded or raked. Another significant factor in feed preservation is the dry matter content (Horrocks *et al.* 1999).

MATERIAL AND METHODS

The field experiment took place in the 2022 season during the second cutting. Basic data on a field where measurements were done: the locality Orlicke Zahori (50.2733097N, 16.4774756E) north-eastern part of the Czech Republic, altitude of 672 m a.s.l. Meteorological conditions during the field experiment are shown in the Table 1.

Table 1 Meteorological conditions
Tabuľka 1 Meteorologické podmienky

Day	26th Aug	27th Aug	28th Aug	29th Aug	30th Aug
Average temperature[1)] [ºC]	23,85	20,65	18,51	18,77	17,91
Rainfall[2)] [mm]	6,3	0	11,1	0	0

[1)]Priemerná teplota, [2)]Zrážky

The measurements were conducted on an experimental, which was divided into four sections (A, B, C, D) of 600 m^2. The first two sections (A, B) were cut with a drum mower without conditioner ZTR 215 of working width 2.15 m. The third and fourth sections (C, D) were mowed with a disc mower with conditioner KUHN FC 1025 F and KUHN FC 8830 D of working width 8.73 m.

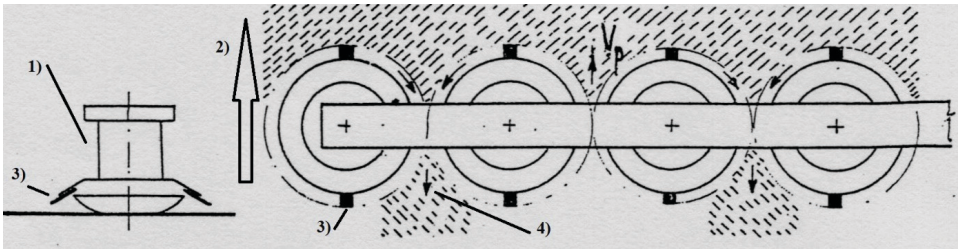

Fig. 1 Scheme of drum mower without conditioner
Obr. 1 Schéma bubnového žacieho stroja bez kondicionéra

[1)]Drum mower, [2)]Direction of tractor driving, [3)]Rotary cutting blade, [4)]Direction of blades rotation
[1)]Bubnový žací stroj, [2)]Smer jazdy traktora, [3)]Žací nôž, [4)]Smer rotácie žacích nožov

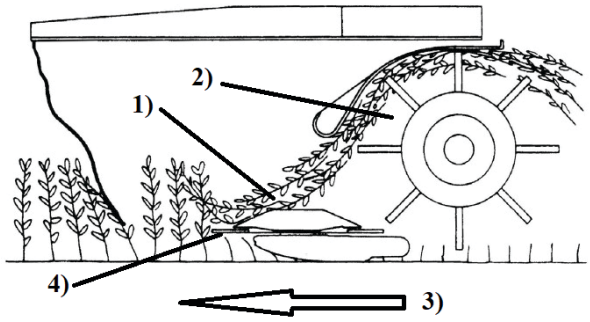

Fig. 2 Scheme of disc mower with conditioner
Obr. 2 Schéma diskového žacieho stroja s kondicionérom

[1)]Disc mower, [2)]Conditioner, [3)]Direction of tractor driving, [4)]Rotary cutting blade
[1)]Diskový žací stroj, [2)]Kondicionér, [3)]Smer jazdy traktora, [4)]Žací nôž

The field experiment is divided into two research parts. The first part is focused on comparing the effect of mowing with conditioner. In this case, for the first two samplings (26th and 28th August) are important samples from section A and section C. The second research part is focused on effect of the number of tedding on the drying process of forage. For samplings in this part (29th and 30th), samples from all sections (A, B, C and D) are major. After mowing (26th August), the first samples of forage from A and C sections were taken to measure the dry matter content. On the third day (28th August), all sections were tedded for the first time. The samples were taken from section A and C. On the fourth day (29th August) only the sections B and D were tedded and from all sections were taken samples. On the fifth day (30th August), all sections were tedded once again. The samples were taken from all sections. For better orientation of the experiment, the individual steps are shown in the Table 2.

Table 2 Overview of the individual works on the given sections
Tabuľka 2 Prehľad jednotlivých prác na daných úsekoch

Section	Drum mower	Disc mower with conditioner	Tedding -28th Aug	Tedding -29th Aug	Tedding -30th Aug
A	X		X		X
B	X		X	X	X
C		X	X		X
D		X	X	X	X

Fig. 3 View of the experimental field during cutting on 26th August
Obr. 3 Pohľad na experimentálne pole počas kosenia 26. augusta

Fig. 4 View of the experimental field during tedding on 28th August
Obr. 4 Pohľad na experimentálne pole počas obracania 28. augusta

Fig. 5 Forage samples taken on 29th August
Obr. 5 Vzorky odobrané 29. augusta

Fig. 6 View of the experimental field with forage samples taken on 30th August
Obr. 6 Pohľad na experimentálne pole s odobratými vzorkami krmoviny 30. augusta

Fig. 7 Aluminium trays with forage samples prepared for drying
Obr. 7 Hliníkové vaničky so vzorkami krmovín prípravenými na dosúšenie

The samples were packed in microtene bags and then placed in leak-proof plastic bags. The evaluation of dry matter content was obtained from the dried residual weight of the forage sample (1). The samples were placed in aluminium trays that had been dried and weighed. Afterwards, the trays were weighed and placed in a heated drying oven. The drying process was conducted at a temperature of 105 ºC. The drying time varied between 2 and 4 hours, depending on the weight and moisture content of the sample. After drying the sample thoroughly, it was important to weigh it quickly to prevent the forage from absorbing moisture from the air, which could lead to measurement inaccuracies. Data were processed by the programmes MS Excel (Microsoft Corp., USA) and Statistica 14 (Statsoft Inc.,USA).

$$x = \frac{m_w - m_d}{m_w} \cdot 100, \quad (1)$$

where x is moisture content of the forage sample [%],
m_w is weight of the wet forage sample [g],
m_d is weight of the dried sample [g].

RESULTS

The first results of the field experiment are a comparison of the dry matter content of forage cut by two types of mowing machines during the drying process. The observed results of the average moisture content of forage samples are shown in the Table 3 and results of the dry matter content are shown in the Figure 3. Tukey´s HSD test (honestly significant difference) indicates that at least one group differs from the other groups. The main idea is to compute the honestly significant difference between two means using a statistical distribution defined by Student and called the q distribution. This distribution gives the exact sampling distribution of the largest difference between a set of means originating from the same population. Boxplot graphs are constructed as arithmetic mean, standard deviation and 0.95-confidence interval. A statistically significant difference in dry matter content was observed for the compared samples from sections B and D of the third measurement (29th August). The results of the Tukey's HSD test are shown in the Fig. 1. For the last fourth measurement (30th August), there was no statistically significant difference in the dry matter content.

Furthermore, the results of the effect of the number of tedding on the drying process of forage were evaluated. Forage samples from sections B and D that were tedded more times showed on average higher values of the dry matter content in comparison to sections A and C. However, statistically significant difference was observed in the samples taken for the third measurement (29th August) from section D. The results of the Tukey's HSD test that proved the statistically significant difference between section C and D are shown on the Fig. 2

Table 3 Average moisture content
Tabuľka 3 Priemerný obsah vlhkosti

Day	Moisture content[1)] [%] section A	Moisture content [%] section B	Moisture content [%] section C	Moisture content [%] section D
26th Aug	61,2	-	61,8	-
28th Aug	55,2	-	56,0	-
29th Aug	34,8	33,2	34,2	31,3
30th Aug	27,7	27,1	26,6	24,5

[1)]Obsah vlhkosti

Tukey HSD test; variable Dry matter content [g·kg^{-1}]
Homogenous Groups, alpha = ,05000
Error: Between MS = 378,27, df = 4,0000

Section	Dry matter content [g/kg]	1	2
B	667,5732	****	
D	686,7174		****

Fig. 8 Tukey's HSD test for section B, D on 29th August
Obr. 8 Tukeyov HSD test pre sekcie B, D 29. augusta

Tukey HSD test; variable Dry matter content [g·kg^{-1}]
Homogenous Groups, alpha = ,05000
Error: Between MS = 378,27, df = 4,0000

Section	Dry matter content [g/kg]	1	2
C	658,0343	****	
D	686,7174		****

Fig. 9 Tukey's HSD test for section C, D on 29th August
Obr. 9 Tukeyov HSD test pre sekcie C, D 29. augusta

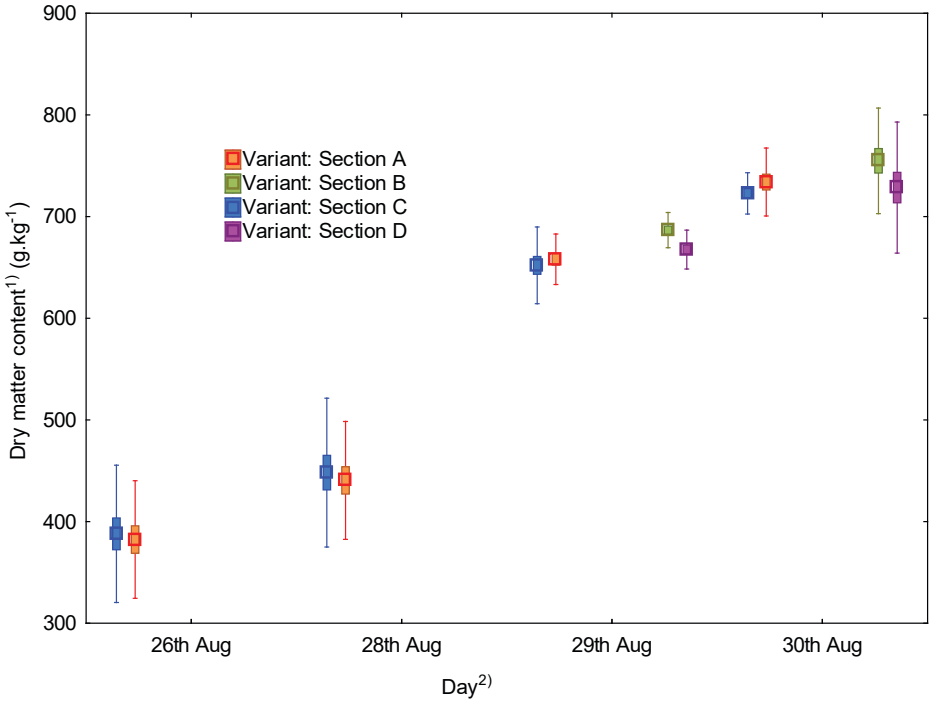

Fig. 10 Observed dry matter content of samples from individual sections
Obr. 10 Zistený podiel obsahu sušiny vzoriek z jednotlivých sekcií
[1]Podiel obsahu sušiny, [2]Deň

DISCUSSION

Rotz *et al.* (1985) list conditions that affect the drying rate of forage. The drying rate is primarily affected by solar insolation. They mentioned also other factors which influenced drying included dry bulb temperature or vapor pressure deficit, soil moisture content, and swath density. Shinners *et al.* (2017) compared various methods of conditioning and tedding forage. The field experiment took place under similar temperature conditions. However, during their field experiment did not occur any rainfall, the moisture content of forage was on the third day below 15%. Due to the rainfall and relatively high air humidity, the observed drying rate corresponded to their drying rate of conditioned forage without tedding. Li *et al.* (2019) evaluated effect of tedding time and frequency on the drying rate of forage. They reached similar results when more times tedded forage showed higher moisture loss during drying. Pattey *et al.* (1988) found out more efficient to ted forage at a lower dry matter content. It corresponds to observed drying process. It is evident from the Figure 3 that the greatest moisture loss was after first tedding on 28th August. Compared to other researches, in this case, under the given conditions, there was no significantly faster drying process of forage that was cut with a conditioner and turned more times compared to unconditioned and less turned forage.

CONCLUSION

1. The results of the comparison conditioned and unconditioned forage proved on average the higher moisture loss at conditioned forage. The differences in some cases were statistically significant.
2. The forage that was more time tedded showed on average higher moisture loss. The observed differences were on the border of statistical significance.
3. Additionaly from the point of view of the economic balance under the given conditions, it would be more appropriate to use a less energy-demanding option (variant A). Mowers equipped with a conditioner have a higher energy demand per hectare. In addition, the number of operations (number tedding) must be included. Given the results found, using the more energy-demand option did not significantly speed up the forage drying process.

REFERENCES

CEMPÍRKOVÁ, R., ČERMÁK, B. 2008. *Krmiva konvenční a ekologická: Feedstuffs conventional and ecological : vědecká monografie*. V Českých Budějovicích: Jihočeská univerzita, Zemědělská fakulta, 2008. ISBN 978-80-7394-141-3

HORROCKS, R. D., VALENTINE, J. F. 1999. *Harvested forages*. Academic Press. ISBN 978-0123562555

LI, Y. W., et al. Effect of Tedding Time and Frequency on the Feed Value and Drying Rate of Rye (Secale cereale L.) Hay. *Journal of The Korean Society of Grassland and Forage Science,* 2019, 39.3: 171-177.

MAŠEK, J., NOVÁK, P. 2011. Technologie sklizně a konzervace krmiv. *Zemědělec* [online]. [cit. 2023-01-10]. Available on: <https://zemedelec.cz/technologie-sklizne-a-konzervace-krmiv/>

PATTEY, E., SAVOIE, P., DUBE, P. A. 1988. The effect of a hay tedder on the field drying rate. *Can. Agric. Eng,* 30.1: 43-50.

ROTZ, C. A., SHINNERS, K. J., BARNES, R. F. 2007. Hay harvest and storage. *Forages*, 2: 601-616.

ROTZ, C. A., CHEN, Y. 1985. Alfalfa drying model for the field environment. *Transactions of the ASAE*, 28.5: 1686-1691.

SHINNERS, K. J., FRIEDE, J. C. 2017. Enhancing Switchgrass Drying Rate. *BioEnergy Research,* 10: 603-612.

Corresponding author:
Libor Matyáš, +420731056235, matyasl@tf.czu.cz

DEVELOPMENT AND PROGRAMMING OF A THERMAL VISION CAMERA USING THE MLX90640 SENSOR: TECHNICAL ASPECTS AND APPLICATIONS IN DRIVER SAFETY

VÝVOJ A PROGRAMOVANIE TERMOVÍZNEJ KAMERY POMOCOU SNÍMAČA MLX90640: TECHNICKÉ ASPEKTY A APLIKÁCIE V OBLASTI BEZPEČNOSTI VODIČA

Rastislav Kollárik[1], Ivan Vitázek[2]

[1]Institute of Agricultural Engineering, Transport and Bioenergetics, Slovak University of Agriculture Tr. A. Hlinku 2, 94976, Nitra, Slovakia, xkollarik@uniag.sk
[2]Institute of Agricultural Engineering, Transport and Bioenergetics, Slovak University of Agriculture Tr. A. Hlinku 2, 94976, Nitra, Slovakia, ivan.vitazek@uniag.sk

ABSTRACT: In today's era, it is crucial to monitor and optimize the microclimate of the interior environment to enhance the comfort and safety of drivers and passengers. When adjusting the parameters of the cabin microclimate, several factors come into play, which affect the health and safety of the passengers, such as the time and attention devoted to parameter settings, as well as the selected parameters themselves. This article focuses on the design, implementation, and testing of an infrared (IR) sensor integrated with an ESP32 module for monitoring the surface temperature of the driver's face in the vehicle. The goal is to analyse the rate of temperature change and optimize the airflow speed and temperature from the vehicle's air conditioning system outlets. The left lower area of the rearview mirror was chosen for sensor placement to capture the largest possible area of the face without obstructing the driver's view. The MLX90640 sensor with a resolution of 32 x 24 pixels was selected for its ability to record temperatures ranging from -40 °C to 300 °C. Connection to other components was established via the I2C protocol. For signal processing from the sensor, the ESP32 microcontroller from Laskakit, featuring Wi-Fi and Bluetooth capabilities, was chosen. Programming was done using Arduino source code, and the results were processed using Processing code. Measurements included experiments with various airflow speeds and their impact on the surface temperature of the driver's face. The results revealed a positive correlation between airflow speed and the rate of temperature change. This finding has the potential to increase the comfort and safety of drivers and passengers in the vehicle. In conclusion, the potential of infrared sensors in future intelligent vehicles is emphasized, highlighting their contribution to optimizing the microclimate and enhancing the comfort and safety of drivers and passengers.

Keywords: microclimate, infrared thermography, thermal comfort, HVAC

ABSTRAKT: V súčasnosti je dôležité sledovať a optimalizovať mikroklímu vnútorného prostredia vozidiel s cieľom zvýšiť pohodlie a bezpečnosť vodičov a cestujúcich. Pri nastavovaní parametrov mikroklímy v kabíne sa stretávame s viacerými faktormi, ktoré ohrozujú zdravie a bezpečnosť posádky, ako je čas a pozornosť venovaná nastaveniu parametrov a samotné vybrané parametre. Tento článok sa zameriava na návrh, implementáciu a testovanie infračerveného (IR) senzora integrovaného s modulom ESP32 na monitorovanie teploty povrchu tváre vodiča vozidla. Cieľom je analyzovať rýchlosť zmeny teploty a optimalizovať rýchlosť prúdenia vzduchu a teploty z výstupov klimatizačného systému vozidla. Pre umiestnenie senzora bol zvolený ľavý spodný roh spätného zrkadla s cieľom zachytiť čo najväčšiu plochu tváre bez obmedzenia vodičovho výhľadu. Senzor MLX90640 s rozlíšením 32x24 pixelov bol vybraný pre svoje schopnosti zaznamenávať teploty v rozsahu od -40 °C do 300 °C. Prepojenie s ostatnými komponentami bolo zabezpečené prostredníctvom I2C protokolu. Na spracovanie signálov zo senzora bol zvolený mikrokontrolér ESP32 od značky Laskakit, ktorý disponuje funkciou Wi-Fi a Bluetooth. Programovanie prebehlo pomocou zdrojového kódu pre Arduino a spracovanie výsledkov pomocou kódu pre Processing. Merania zahŕňali aj experimenty s rôznymi rýchlosťami prúdenia vzduchu a ich vplyvom na zmenu teploty povrchu tváre vodiča. Výsledky ukázali pozitívnu koreláciu medzi rýchlosťou prúdenia vzduchu a rýchlosťou zmeny teploty. Tento poznatok má potenciál zvýšiť komfort a bezpečnosť vodiča a cestujúcich vo vozidle. V závere sa zdôrazňuje potenciál infračervených senzorov v inteligentných vozidlách budúcnosti a ich prínos pri optimalizácii mikroklímy a zvýšení komfortu a bezpečnosti vodičov a cestujúcich.

Kľúčové slová: mikroklíma, infračervená termografia, tepelná pohoda, HVAC

INTRODUCTION

In recent years, the development and application of thermal vision technology have significantly advanced, offering numerous benefits in various fields, including driver safety. Monitoring and optimizing the microclimate inside a vehicle is essential for enhancing the comfort and safety of both drivers and passengers. Current solutions in this domain involve sophisticated technologies that provide real-time data on temperature, humidity, and airflow, contributing to the overall driving experience.

A variety of approaches have been explored to address the challenges associated with maintaining an optimal cabin environment. For instance, studies by (Yi et al. 2020) and (Ugursal et al. 2012) have demonstrated the effectiveness of using infrared (IR) sensors to monitor and regulate the temperature inside vehicles. These studies have shown that precise temperature monitoring can significantly improve the comfort and alertness of drivers, thereby reducing the risk of accidents caused by discomfort or fatigue.

The MLX90640 IR sensor, with its high resolution and broad temperature range, has emerged as a reliable tool for such applications. The sensor's ability to measure temperatures from -40 °C to 300 °C and its 55° field of view make it ideal for capturing detailed thermal images of the driver's face. The integration of this sensor with microcontrollers, such as the ESP32, allows for efficient data processing and transmission, facilitating real-time monitoring and control of the vehicle's microclimate.

Existing research highlights the potential of these technologies to enhance driver safety. For example, the work by (Shin et al. (2017) illustrated the use of thermal imaging to detect signs of driver fatigue by monitoring facial temperature changes. Similarly, (Vavrinsky et al. (2013) explored the use of IR sensors to optimize HVAC (Heating, Ventilation, and Air Conditioning) systems in vehicles, leading to improved energy efficiency and passenger comfort.

This study builds upon these findings by focusing on the design, implementation, and testing of a IR vision system using the MLX90640 sensor. The system aims to monitor the surface temperature of the driver's face and adjust the airflow and temperature from the vehicle's air conditioning system to maintain optimal comfort. The sensor is strategically placed in the lower left area of the rearview mirror to capture the largest possible area of the face without obstructing the driver's view.

The microcontroller chosen for this project is the versatile Laskakit ESP32-Lpkit, which offers built-in Wi-Fi and Bluetooth modules, making it suitable for a wide range of applications, from low-power sensor networks to demanding processing tasks. The programming of the system was done using Arduino source code, and the data visualization was achieved using Processing code.

By conducting experiments with varying airflow speeds, this study aims to analyse the rate of temperature change on the driver's face. The results are expected to demonstrate a positive correlation between airflow speed and temperature regulation, thereby validating the effectiveness of the proposed system. Ultimately, this research aims to contribute to the development of intelligent vehicles that use advanced thermal vision technology to enhance driver and passenger safety and comfort.

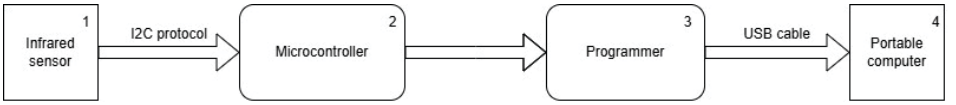

Fig.1 Block scheme of a device
Obr.1 Bloková schéma zariadenia

MATERIAL AND METHODS

Infrared sensor MLX90640

The MLX90640 is an infrared sensor with a resolution of 32 x 24 pixels, capable of measuring temperatures ranging from -40 °C to 300 °C. The sensor's field of view is 55°, and its coverage, when placed in a specified location, is focused on the head area of a person with sufficient overlap, as shown in Figure 3. Connection to other devices is established through the I2C protocol. The sensor can be powered with two configurations, 3,3 V and 5 V, making it energy-efficient.

Microcontroller Laskakit ESP32 – Lpkit

The microcontroller from Laskakit was chosen for processing signals from the sensor. This is a versatile microcontroller with built-in Wi-Fi and Bluetooth modules. It is designed for various applications, from low-power sensor networks to demanding tasks. It is based on the ESP32-DOWDQ6 chip with two independent CPU cores. The CPU frequency is adjustable from 80 MHz to 240 MHz. The module supports data transfer rates of up to 150 Mbps and an antenna output power of 20 dBm. The operating current is 80 mA, and the voltage ranges from 3 to 3.6 V.

Programmer LaskaKit CH90102

The universal programmer with the USB-UART converter CH9102 is designed for uploading firmware to development boards, including those from LaskaKit. It is a simple and affordable device that can be used with boards containing ESP or Atmel chips. The power supply can be set to 3,3 V or 5 V. The programmer supports microUSB or USB-C connectors for connection to devices.

Datalogger AHLBORN ALMEMO 2590-4AS

The datalogger is a device for collecting and storing data, featuring a total of four inputs, sixteen channels (+4 internal channels) with a maximum permissible measurement error of ±0,03 %, placing it in accuracy class A. Measured values are displayed digitally on a graphic LCD with a resolution of 128 x 64 pixels. The datalogger's memory can store up to 100000 measured values and can be powered by three AA batteries or an AC adapter. The interface is provided through USB 2.0, RS232, Ethernet, or Bluetooth. Data recorded by the device can be processed in AHLBORN's software to create graphical or tabular evaluations of the values. The measurement rate can be selected between 10 and 2,5 Hz.

Airflow Velocity Probe ALMEMO FVAD S120

For measuring airflow velocity, we used the ALMEMO FVAD 15 S120 probe connected to the ALMEMO 2590-4AS datalogger, with a measurement range from 0,4 to 20 m/s and an accuracy of ±1,5 % of the measured value. Measurements can be performed at temperatures ranging from -20 to 140 °C.

Temperature, Atmospheric Pressure, and Relative Humidity Probe ALMEMO FHAD 46-C2

Probe can measure ambient temperature, relative humidity, atmospheric pressure, and dew point in each space. It is used exclusively with the ALMEMO 2590-4AS datalogger, which displays the current values of all four parameters in real-time upon connection. The measurement accuracy for relative humidity is ±2 % in the first range (10 ÷ 90 %) or ± 4 % in the second range (5 ÷ 98 %). The temperature measurement range is from -20 to 60 °C.

Arduino Source Code

Arduino code is used for reading images from the MLX90640 IR sensor, which communicates via the I2C interface with the ESP32 microcontroller, specifically with the Laskakit ESP32-LPKIT development board. Initially, the code includes the necessary library for communication with the thermal camera. It then declares an object for the thermal camera and arrays to store temperature data for each pixel and compressed messages.

In the `setup()` function, which runs after startup, the code initializes serial communication at 500000 baud and waits a short time to stabilize communication. Then it attempts to initialize the thermal camera at its default I2C address and sets the emissivity (0,96). If the camera is not found, it prints an error message and stops the program. If the camera is successfully found, the code prints basic information about the thermal camera, such as its I2C address and serial number.

It then sets the scanning mode to "interleaved chessboard" or "interleaved rows,"

the ADC resolution, which affects the accuracy of temperature measurements, and the camera's refresh rate, which determines how often new temperature images are provided. The `loop()` function, which repeats continuously, attempts to read an entire image from the thermal camera. If an error occurs, it prints an error message and skips the current cycle. If the image is successfully read, the code compresses the temperature data into 16-bit values and stores them in the message array along with a unique "MAGIC" value at the beginning.

These compressed temperature data are then sent via the serial link to the computer. The code also checks for any commands from the computer to set the camera's refresh rate and makes the corresponding change if necessary. This way, the code enables the capture of temperature data using the MLX90640 thermal camera, its processing, and sending it to the computer, while allowing dynamic adjustment of the camera's refresh rate based on commands from the computer.

Processing Source Code

Processing language is used to visualize temperature data from images obtained using the thermal camera, which are transmitted via the serial link (USB). Initially, the code imports the library for working with serial communication and declares several global variables. It defines the size of temperature cells in pixels, the serial port, and a two-dimensional array to store temperature data. Additionally, helper variables are initialized to track the minimum, maximum, and average temperature in the image, alarm and its filter, coordinates of cells with minimum and maximum temperatures, and other variables for various functions.

In the `setup()` function, the basic window configuration, colour model, serial port, and other initializations are set. It attempts to open the serial port on the first available port at 500000 baud. If opening the port fails, it prints an error message and terminates the program. The code also sets a custom cursor in the shape of a crosshair. In the `draw()` function, it continuously attempts to read new data from the serial port unless the program is paused. If new data is available, it updates the window title, clears the background, draws the image, optionally applies a blur, and draws crosshairs on the cells with minimum and maximum temperatures. It also displays temperature statistics and exports these data to a file. If the mouse moves over any of the cells, it displays the temperature of that cell at the cursor. In the `mouseMoved()` function, the mouse cursor position is updated only if a sufficient time interval has passed. The smooth cursor position and coordinates of the cell under the cursor are updated. In the `exportStatistics()` function, statistical data are written to a file. The `keyPressed()` function allows various interactions via the keyboard, such as changing the pause state, showing or hiding text at the cursor, changing the size of temperature cells, setting the camera's refresh rate, and exporting statistics. In the `readImage()` function, data from the serial port are processed and stored in the two-dimensional temperature data array.

The average temperature, maximum and minimum temperatures, and their coordinates are updated. The median temperature is also calculated. In the `drawImage()` function, temperature data are drawn as coloured squares in the window. The `drawExtremeCross()` function draws crosshairs and temperature values on the cells with maximum and minimum temperatures. The `drawStatistics()` function displays statistical data such as minimum,

average, median, and maximum temperatures at the bottom of the window. If the alarm is activated, a warning message is displayed. Finally, the `calculateMedian()` function calculates the median of the values in the temperature array.

Placement of IR Sensor

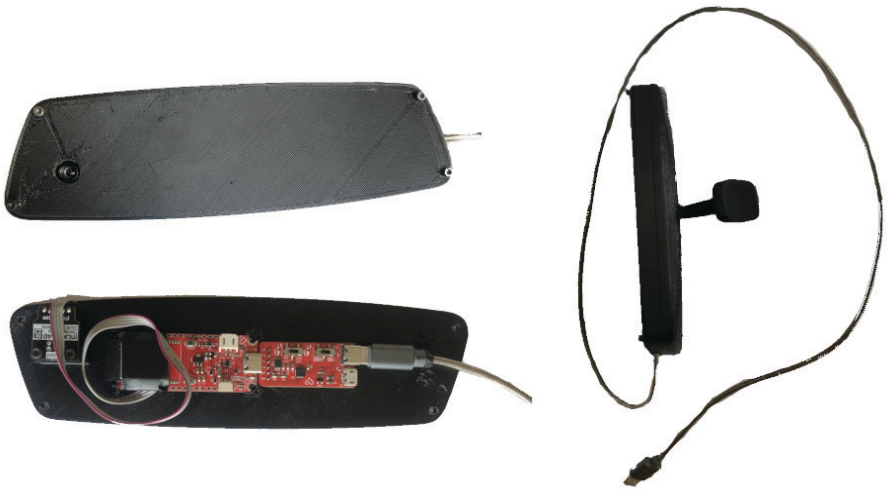

Fig.2 Infrared device inside of a rearview mirror model
Obr.2 Infračervené zariadenie vo vnútri modelu spätného zrkadla

The placement of the infrared sensor in the lower left corner of the rearview mirror as shown in Figure 2, was chosen to capture the largest possible area of the face while not obstructing the driver›s field of view. Figure 3, shows the car schematic with the field of view highlighted. The entire setup consists of three main components: the infrared sensor, microcontroller, and programmer.

Fig.3 Visualization of IR sensor field view inside a vehicle
Obr.3 Vizualizácia zorného poľa IR snímača vo vozidle

RESULTS

Table 1 presents the median temperatures recorded during three separate measurements, each conducted at different fan speed settings (first, second, and third). The measurements were taken at 10-second intervals, up to 110 seconds.

Across all three measurements, the initial temperatures were similar for each fan speed. There was a rapid decrease in temperature within the first 20 seconds for all fan speeds, followed by stabilization. The third fan speed stage generally resulted in a lower stabilization temperature compared to the first and second stages. The first fan speed stage consistently showed a higher final median temperature compared to the second and third stages, indicating that higher fan speeds are more effective at reducing temperatures.

Table 1 The progression of changes in median temperature values recorded during three measurements, depending on the selected fan speed setting
Tabuľka 1 Vývoj zmien v hodnotách mediánu teplôt zaznamenaných počas troch meraní v závislosti od nastaveného stupňa ventilátora

Median of temperature from first measurement[1] [°C]				Median of temperature from second measurement[2] [°C]				Median of temperature from third measurement[3] [°C]			
Time[4] [s]	First stage of fan speed[5]	Second stage of fan speed[6]	Third stage of fan speed[7]	Time[4] [s]	First stage of fan speed[5]	Second stage of fan speed[6]	Third stage of fan speed[7]	Time[4] [s]	First stage of fan speed[5]	Second stage of fan speed[6]	Third stage of fan speed[7]
0	31,60	31,80	30,80	0	31,60	31,80	31,40	0	31,51	31,71	30,67
10	29,58	28,70	28,63	10	29,58	28,70	28,63	10	29,59	28,70	28,84
20	29,07	28,00	28,00	20	29,07	28,00	27,83	20	29,23	28,11	27,98
30	28,80	27,79	27,84	30	28,80	27,79	27,64	30	28,92	27,95	27,95
40	28,66	27,68	27,34	40	28,66	27,68	27,34	40	28,54	27,63	27,31
50	28,36	27,63	27,35	50	28,36	27,93	27,35	50	28,27	27,68	27,41
60	28,05	27,48	27,28	60	28,05	27,48	27,28	60	28,02	27,55	27,24
70	27,96	27,40		70	27,96	27,40		70	27,85	27,44	
80	27,94			80	27,94			80	27,96		
90	27,85			90	27,85			90	27,64		
100	27,67			100	27,67			100	27,81		
110	27,62			110	26,62			110	27,44		

[1]Medián teplôt z prvého merania A, [2]Medián teplôt z druhého merania B, [3]Medián teplôt z tretieho merania C, [4]Čas, [5]Prvý stupeň rýchlosti ventilátora 1, [6]Druhý stupeň rýchlosti ventilátora 2, [7]Tretí stupeň rýchlosti ventilátora 3

Figures 4 through 7 show the time-dependent temperature curves for different fan speed settings of the interior fan. The curves are described by trend lines with corresponding equations for all variants and measurements. In the first series of measurements, the lowest achievable temperature of 27 °C was reached within 110 seconds at the first fan speed setting. At the second fan speed setting, this temperature was reached within 70 seconds. At the third, maximum fan speed setting, the local minimum temperature was achieved within 60 seconds.

In the second series of measurements, the lowest achievable temperature of 27 °C was reached within 110 seconds at the first fan speed setting. At the second fan speed setting, this temperature was reached within 70 seconds. At the third fan speed setting, the minimum temperature was achieved within 60 seconds.

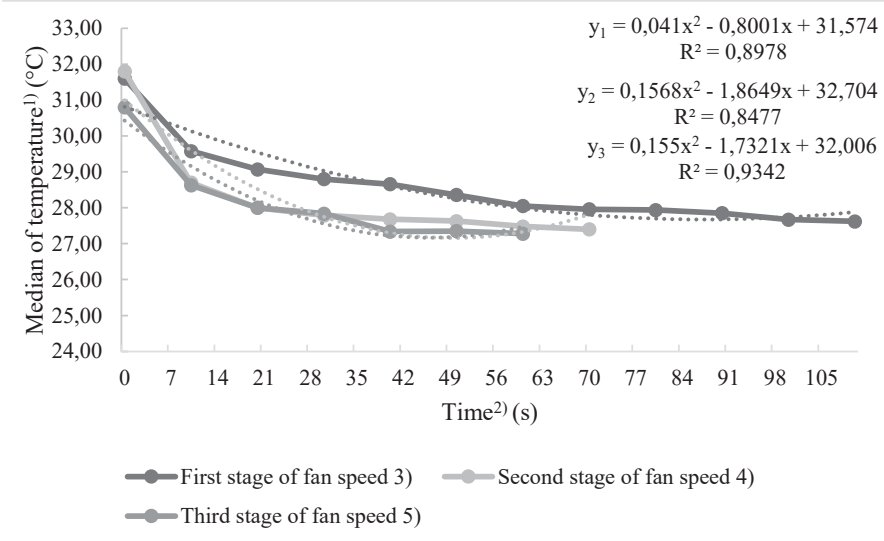

Fig.4 Graphical representation of Table 1 for the first measurement
Obr.4 Grafické spracovanie tabuľky 1 pre prvé meranie

[1)]Medián teplôt, [2)]Čas, [3)]Prvý stupeň rýchlosti ventilátora, [4)]Druhý stupeň rýchlosti ventilátora, [5)]Tretí stupeň rýchlosti ventilátora

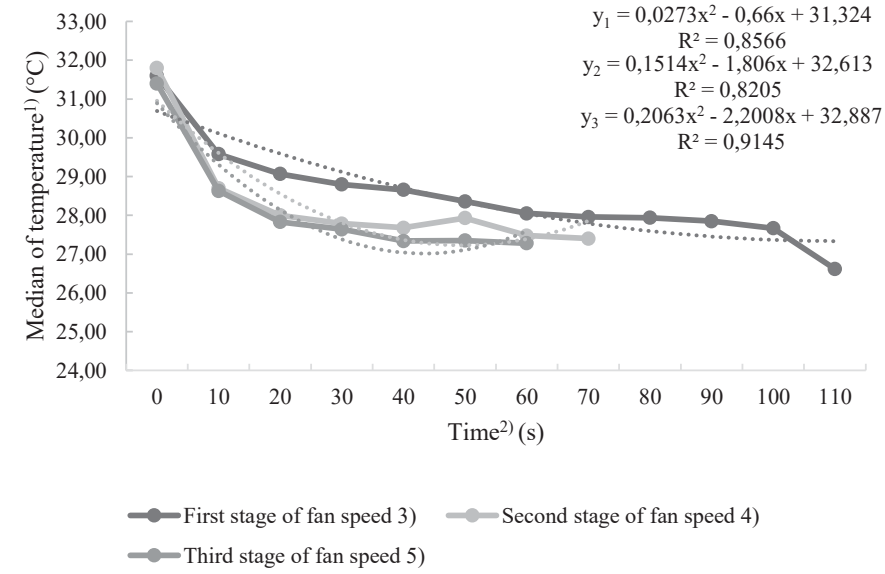

Fig.5 Graphical representation of Table 1 for the second measurement.
Obr.5 Grafické spracovanie tabuľky 1 pre druhé meranie

[1)]Medián teplôt, [2)]Čas, [3)]Prvý stupeň rýchlosti ventilátora, [4)]Druhý stupeň rýchlosti ventilátora, [5)]Tretí stupeň rýchlosti ventilátora

In the final, third series of measurements, the lowest achievable temperature was reached within 110 seconds at the first fan speed setting. At the second fan speed setting, this temperature was reached within 70 seconds. At the third fan speed setting, the minimum temperature was achieved within 60 seconds.

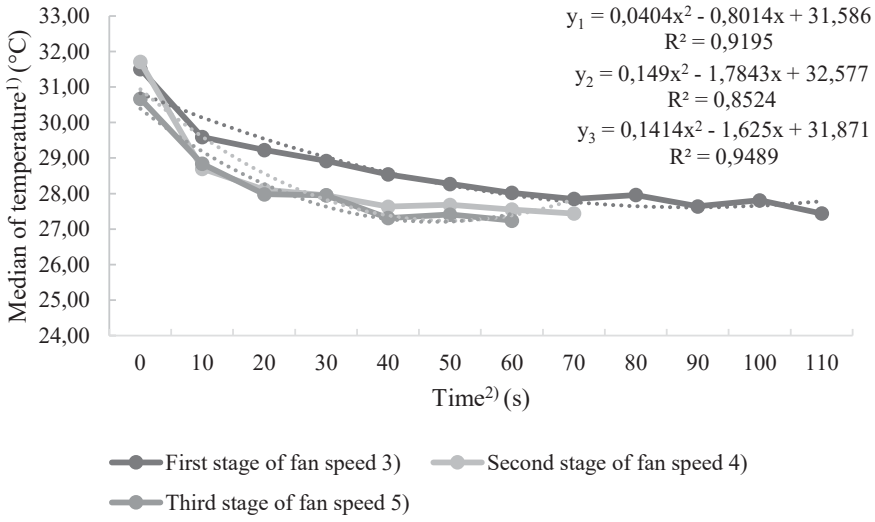

Fig.6 Graphical representation of Table 1 for the third measurement.
Obr.6 Grafické spracovanie tabuľky 1 pre tretie meranie
[1)]Medián teplôt, [2)]Čas, [3)]Prvý stupeň rýchlosti ventilátora, [4)]Druhý stupeň rýchlosti ventilátora, [5)] Tretí stupeň rýchlosti ventilátora

Pearson's correlation analysis demonstrated a very strong relationship between the measured values across different fan speed settings, as shown by the heat map in Figure 7. he R values for all measurements were greater than 0,96.

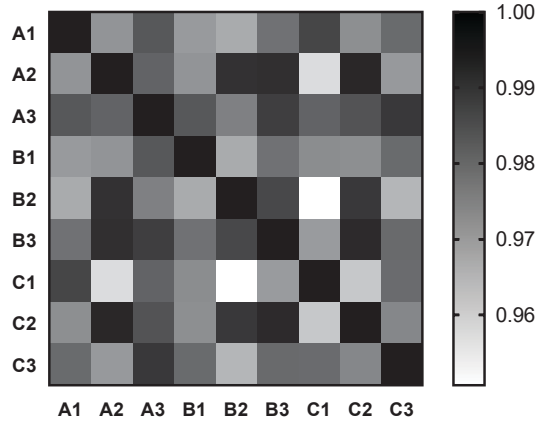

Fig.7 Pearson correlation of measurements in heat map
Obr.7 Pearsonova korelácia pre namerané hodnoty zobrazená v heat map

DISCUSSION

By evaluating the results of measurements of the median value of the surface temperature of the face under changing air flow conditions, we can conclude that with increasing air flow speed, the surface temperature of the subject's face cools down faster than at lower airflow speeds. A similar pattern is described by Koukiou and Anastassopoulos; utilizing the time dependency of temperature changes can distinguish the fan speed setting of the HVAC unit.

The choice of HVAC fan speed depends on the current microclimate conditions of the environment as well as the thermal comfort preferences of the subject. The device described above is designed to monitor the rate at which the surface temperature of the subject's face changes. In an enclosed environment, this rate is influenced by the humidity, the magnitude of temperature changes, and the airflow speed which also described Zhou et al.. In a broader context, this device is purposefully designed for a system capable of evaluating the thermal comfort of a subject in environments with rapidly changing microclimate parameters.

As described by Vitázek, choosing extreme HVAC settings exposes the driver to an increased risk of accidents, long-term health hazards, and, in extreme cases, death, mainly due to heart failure caused by thermal shock. Health and other risks are also described by LEAH.

CONCLUSION

Through experimental measurements in a vehicle, we recorded the surface temperatures of the driver's face using an infrared sensor while varying the air flow speed from the HVAC outlets. During the experiment, we monitored the air flow speed, median temperatures at specific time intervals, and the time required to observe a decrease in temperature from a local maximum to a local minimum, which also represented the overall minimum.

The reliability of the device is indicated by the consistent temperature drop times across all measurements, with the same time period needed to decrease the temperature from the local maximum to the minimum temperature of 27 °C. These findings are further supported by Pearson‘s correlation results, which show a very strong relationship between the measured values, with R values above 0,96. Based on these correlations, the device can be used in vehicles to determine the selected fan speed setting. This device represents a significant advancement for enhancing the efficiency and accuracy of autonomous climate control in the given environment based on our published work.

ACKNOWLEDGMENT

Grants and companies that have allowed research to be published.

REFERENCES

CIAMPA F., MAHMOODI P., PINTO M. 2018. Recent Advances in Active Infrared Thermography for Non-Destructive Testing of Aerospace Components. In Sensors, vol. 18, p. 609, DOI:10.3390/s18020609.

KOUKIOU G., ANASTASSOPOULOS V. 2015. Neural networks for identifying drunk persons using thermal infrared imagery, In Forensic Science International,vol. 252,2015, pp. 69-76, ISSN 0379-0738, DOI: https://doi.org/10.1016/j.forsciint.2015.04.022.

LEAH H. et al., 2018, Modification of the association between high ambient temperature and health by urban microclimate indicators: A systematic review and meta-analysis, In Environmental Research, vol. 161, 2018, pp. 168-180, ISSN 0013-9351, DOI: https://doi.org/10.1016/j.envres.2017.11.004.

SHIN Y., IM, G., YU K., CHO H. 2017. Experimental study on the change in driver's physiological signals in automobile HVAC system under Full load condition. In Applied Thermal Engineering, vol.112, pp. 1213-1222, ISSN 1359-4311, DOI: 10.1016/j.applthermaleng.2016.10.193.

SURESH P., THEIVADAS R., KUMAR H., ENINARSON D. 2022. Driver monitoring and passenger interaction system using wearable device in intelligent vehicle. In Computers and Electrical Engineering, vol. 103, pp. 108323, ISSN 0045-7906, DOI: 10.1016/j.compeleceng.2022.108323.

UGURSAL A., CULP H. 2012. An Empirical Thermal Comfort Model for Transient Metabolic Conditions. In ASHRAE Transactions, vol. 118, no. 1, pp. 742-750, ISSN 0001-2505.

VITÁZEK I., TKÁČ Z., MAJDAN R. 2021. Interior environment in vehicles: features and their evaluation (in Slovak). 1. Release. Nitra: Slovak University of Agriculture, 2021. Article 133, ISBN 978-80-552-2424-4.

YI X., ZHAOMING L., JIANGYAN L., KUINING L., YANGJUN Z., CUNXUE W., PINGZHONG W., XIAOBO W. 2020. A Self-learning intelligent passenger vehicle comfort cooling system control strategy, In Applied Thermal Engineering, vol. 166, 2020, Article 114646, ISSN 1359-4311, DOI: 10.1016/j.applthermaleng.2019.114646.

YUE Y., YUQI H., JISHENG Z. 2020. Optimization of the automotive air conditioning strategy based on the study of dewing phenomenon and defogging progress, In Applied Thermal Engineering, vol. 169, 2020, Article 114932, ISSN 1359-4311, DOI: 10.1016/j.applthermaleng.2020.114932.

ZHOU X., et al., 2023. InfraNet: Accurate forehead temperature measurement framework for people in the wild with monocular thermal infrared camera, In Neural Networks, vol. 166, 2023, pp. 501-511, ISSN 0893-6080, DOI: https://doi.org/10.1016/j.neunet.2023.07.038.

Corresponding author:
Rastislav Kollárik, tel. +421 905 768 881, e-mail: xkollarik@uniag.sk

EFFICIENCY OF MANUAL SORTING PLANTS FOR PLASTIC WASTE

ÚČINNOSŤ RUČNÝCH TRIEDIČIEK PLASTOVÉHO ODPADU

Jan ŠONSKÝ[1], Petr Vaculík[1], Vlastimil Altmann[2] , Shuran Zhao[2]

[1]Department of Technological Equipment of Buildings, Faculty of Engineering, Czech University of Life Sciences Prague, Kamýcká 129, 165 21 Prague, Czech Republic,
[2]Department of Machinery Utilization, Faculty of Engineering, Czech University of Life Sciences Prague, Kamýcká 129, 165 21 Prague, Czech Republic,

ABSTRACT: Waste management is an integral part of people's lives. With the overall growth in wealth and population, the amount of waste that society produces is increasing. A frequently mentioned type of waste is plastic waste, which is generated by people's daily activities. Thus, plastic waste forms an integral part of municipal waste. Despite the very high percentage of people who sort plastics in the Czech Republic, the recycling of plastics does not reach similarly high percentages. An important precursor to recycling, and an intermediate step after sorting by citizens, are sorting plants. These plants sort plastics into different types, mainly polyethylene terephthalate (PET), polypropylene (PP) and polyethylene (PE). With three exceptions, sorting of plastics in the Czech Republic is carried out manually, with the help of operators who pull the different types of plastics from a conveyor belt. Manual sorting has its physical limits, and as the capacity of the input waste increases, the sorting efficiency decreases, which has a major impact on the economics of the entire plant. Despite the impossibility of knowing the type of plastic, these plants achieve desirable yields of plastics for recycling. In view of the rising cost of human labour and low unemployment, it can be predicted that manual sorting will be gradually reduced in the future and replaced by machine sorting. This phenomenon can also be observed in the more developed countries of the European Union.

Keywords: waste, waste management, waste plastic sorting, plastic

ABSTRAKT: Odpadové hospodárstvo je neoddeliteľnou súčasťou života ľudí. S celkovým rastom bohatstva a počtu obyvateľov sa zvyšuje množstvo odpadu, ktoré spoločnosť produkuje. Často spomínaným druhom odpadu je plastový odpad, ktorý vzniká pri každodenných činnostiach ľudí. Plastový odpad tak tvorí neoddeliteľnú súčasť komunálneho odpadu. Napriek veľmi vysokému percentu ľudí, ktorí v Českej republike triedia plasty, recyklácia plastov nedosahuje podobne vysoké percento. Dôležitým predstupňom recyklácie a medzistupňom po triedení občanmi sú triediace linky. Tieto linky triedia plasty na rôzne druhy, najmä na polyetyléntereftalát (PET), polypropylén (PP) a polyetylén (PE). Až na dve výnimky sa triedenie plastov v Českej republike vykonáva ručne, pomocou operátorov, ktorí jednotlivé druhy plastov sťahujú z dopravníkového pásu. Ručné triedenie má svoje fyzikálne limity a so zvyšujúcou sa kapacitou vstupného odpadu klesá účinnosť triedenia, čo má veľký vplyv na ekonomiku celej linky. Napriek nemožnosti poznať typ plastu dosahujú tieto linky želateľnú výťažnosť plastov určených na recykláciu. Vzhľadom na rastúce náklady na ľudskú

prácu a nízku nezamestnanosť možno predpokladať, že ručné triedenie sa bude v budúcnosti postupne obmedzovať a nahrádzať strojovým triedením. Tento jav možno pozorovať aj vo vyspelejších krajinách Európskej únie.

Kľúčové slová: odpad, odpadové hospodárstvo, triedenie plastového odpadu, plast

INTRODUCTION

Waste management is an integral part of people's daily lives (*Gadaleta et al., 2020*). The amount of municipal waste in the country is on an increasing trend. In 2022, 5.2 million tons of municipal waste was produced. Plastic waste is a significant part of municipal waste. The global production of plastic exceeds 359 million tons per year (*Nayanathara, 2024*). Moreover, production is expected to double in 2045 (*Bergmann et al., 2022*). Plastic waste is one of the most discussed waste commodities in the world. Paradoxically, it accounts for about 1% of all waste in the world (*Dearmitt, 2020*). In the European Union, about 40% of plastics are used for packaging. 20% of plastics are used in construction. 10% of plastics are used in automotive. Only 32.5% of plastic waste was recycled in the EU in 2018. The majority share (42.6%) of the plastic waste load is energy recovery. Up to 25% of plastic waste is landfilled („Plastic Waste and Recycling in the EU: Facts and Figures"). Due to the low degradation of plastics in nature, unsustainable production, frequent use and inadequate management of plastic waste, plastics have become a serious threat to natural ecosystems and human health (*Walker, 2023*) . In the Czech Republic, waste collection is mainly carried out through collection points arranged by municipalities, which have this obligation under the Waste Act. The collection of plastic waste in the Czech Republic started in 1997, with the establishment of an authorised packaging company, which finances the system on the basis of the joint fulfilment of the obligations laid down in Sections 10 to 12a of the Packaging Act No. 477/2001 Coll. The yellow plastic containers are then taken by collection trucks to sorting plants (*Callewaert et al., 2023*).

Sorting plants are an important part of the plastic waste management process. It is an intermediate step between collection and recycling of plastics. The high variety of plastic types ensures that they are difficult to recycle, as each type of plastic has different properties. It is therefore necessary to sort mixed plastics, preferably into individual plastic types or groups of plastics that have similar properties (*Šťastná, 2013*). The sorting of mixed plastics is either manual or automated (*Aschenbrenner et al., 2023*). Manual sorting makes considerable use of human labour. It is a less efficient sorting method than automatic sorting, using various machines. Automated sorting also achieves greater purity of the output material (*Kroell, 2024*). The Waste Management Information System (VISOH2) records 76 active stationary sorting plants for mixed plastic waste in operation in the Czech Republic, accepting waste with catalogue number 20 01 39. Three plants are automated, in Ostrava, Brno and Prague (*Vlkov, n.d.*). Manual sorting plants are the most common way of sorting plastics in the Czech Republic. These plants operate on the same principle (*Lim et al., 2023*). Mixed plastics are transported by collection trucks to the storage section. The waste is piled onto an inlet conveyor which is sunk below ground level. The piling process involves the first stage of manual sorting, i.e. removal of oversized items, i.e. film, carpet, PVC, etc. Oversized pieces of waste would burden the next stage of sorting by

overlapping the waste on the belt. The waste is further taken to the sorting cabin, which is located above the tipping boxes, by means of a conveyor belt. The sorting cab contains the sorting belt and the drop boxes located below the cab. In the sorting cabin, workers remove and therefore positively sort selected types of plastics from the material flow and drop them into the adjacent drop boxes. With regard to the size of the material, the sorting cabin is arranged so that the larger, i.e. bulkier, pieces of plastic are sorted at the beginning. Valuable materials such as PET bottles follow, with a view to possible interception by other workers. Less valuable materials are sorted towards the end of the sorting cabin. Currently the following plastics are sorted: PET bottles, polypropylene and polyethylene plastics, LDPE clear film, LDPE coloured film, HDPE plastics, PVC, beverage cartons (tetrapak), ferrous and non-ferrous metals. Sorted raw materials are stored in boxes under the sorting cabin. Once sufficient quantities are filled, the plastics are manually or mechanically piled onto a recessed conveyor. This conveyor conveys the material to a baling press where it is compacted to reduce storage space and transportation costs (*Roosen et al., 2020*). The baled bales are then transported away for recycling or other uses. Plastic that is not removed from the flow in the sorting booth travels outside the sorting booth and is called reject. This is usually used to produce a solid alternative fuel called RDF (*Tripathi & Rao, 2023*). For proper setup of sorting plants and processes, it is necessary to know the composition of the input waste, i.e. mixed plastics. This is a non-homogeneous mixture that varies over the seasons and is different for different types of developments. In urban developments, the population generates more plastic waste than in rural developments (*Zhang et al., 2023*). *Lahtela et al.*, (2019) states that there are non-plastic wastes in plastic waste that are undesirable for the sorting process.

The aim of this work is to evaluate the yield of manual sorting plants and determine their maximum yield with respect to the amount of waste processed. It can be hypothesized that manual sorting plants have their limits with respect to the physical capacity of humans and it is necessary to gradually replace manual sorting plants with machine plants.

MATERIAL AND METHODS

Four sorting plants in the Czech Republic with different input capacities in one year were analysed. All sorting plants sort the same types of plastics, clear, blue, green and mixed PET bottles, HDPE, PP and PE, coloured LDPE film, clear LDPE film, Tetrapak and PVC. Sorting plants had same number of workers for sorting during year. The individual fractions are recorded as output from the sorting plants in the form of compressed bales which are sold for recycling. Bales are weighted on weighbridge for each fraction after every sorting shift. Every bale has same measure proportion which is set by baler. Same baler is used on all monitored sorting plants, same pressure was set. The weight of the bales was measured at the end of the morning shifts on all sorting plants studied for one year period of time. One year was chosen as the time period to be monitored due to differences in the composition of mixed plastic waste during the year. The remaining fraction, known as reject, is passed on for the production of solid alternative fuel and is weighted in walking floor truck after every retrieval. In order to understand the yield of plastics, an analysis of the composition of the mixed plastics was carried out by self-analysis based on the methodology of research project No. SP/2F1/132/08. Collected data were analyzed in MS Excel and compared. The results were interpreted as tables and graphs.

RESULTS

Table 1 shows the quantity of plastics processed over the period under review and the average recovery of plastics over the period. The highest yield is achieved by plant 4, which also has the lowest input capacity. Plant 3 has the lowest yield of 36,98 % with an average annual input of 2639 tonnes. Plant 3 had the lowest yield, with an annual processed capacity of 2639.63 tonnes. The low yield can be attributed mainly to poor manual sorting, lack of motivation of the employees and the technical background of this plant. Plant 3 is located in a less developed part of the country where fewer people initially sort waste. The area has a higher unemployment rate than the average in the country and it can be inferred that people generate less waste as their purchasing power is weaker than, for example, in the area of plant 1 and 2, where mainly waste from larger cities is processed. *Minelgaitė & Liobikienė, (2019)* describes that the amount of waste or its production strongly depends on the economic level. Table 2 shows that plants with smaller amounts of processed waste achieve higher yields.

Table 1 Input to sorting plants and their annual yield
Tabuľka 1 Vstupy do triediacich liniek a ich ročný výnos

	Annual processed capacity [t/h]	**Average percentage recovery of plastics [%]**
Sorting plant 1	1091,51	61,66 %
Sorting plant 2	2940,82	47,57 %
Sorting plant 3	2639,63	36,98 %
Sorting plant 4	893,76	65,46 %

The individual yield of sorted plastics is monitored on the sorting palnts. The methodology for calculating the yields is the difference between the input quantity and the bales of each type of plastic that are compacted. Compression is carried out to reduce storage capacity and transport costs for recycling. Table 2 shows the average yield of each plastic over the period under review.

Table 2 shows that the most sorted commodity is a mixture of PP and PE and coloured LDPE film. For PP and PE, these are larger pieces of packaging materials, e.g. from pharmaceuticals, washing powders, etc. A smaller part is taken up by yoghurt cups and other food trays. Films are also larger pieces and easily recognisable to people. HDPE plastics, such as garden furniture and children‘s toys, which are not commonly found in plastics, have the lowest yields. The average recovery rate of 50.93% shows that more than half of the plastics that people sort into yellow bins have no recycling potential. Over the course of the year, the recovery of different types of plastics varies with the composition of the input waste. This is dependent on consumer behaviour (Ma et al., 2018), as shown in the following figures.

Table 2 Average yield of each type of sorted plastic
Tabuľka 2 Priemerná výťažnosť každého druhu triedeného plastu

Type of plastic / Sorting plant	Sorting plant 1	Sorting plant 2	Sorting plant 3	Sorting plant 4
PET bottles clear	8,21%	8,74%	7,37%	5,59%
PET bottles blue	1,28%	1,53%	0,23%	1,60%
PET bottles green	1,33%	1,55%	3,78%	1,32%
PET bottles mix colours	6,04%	4,43%	2,32%	4,51%
Tetrapak	0,65%	1,46%	0,44%	2,51%
HDPE	0,66%	0,00%	0,29%	0,00%
LDPE foil clear	5,79%	7,73%	6,06%	11,91%
PP/PE	20,54%	11,77%	8,76%	16,93%
LDPE foil mix colours	15,98%	6,97%	3,74%	15,71%
PVC	1,17%	3,40%	3,99%	5,37%
Total sorted	61,66%	47,57%	36,98%	65,46%

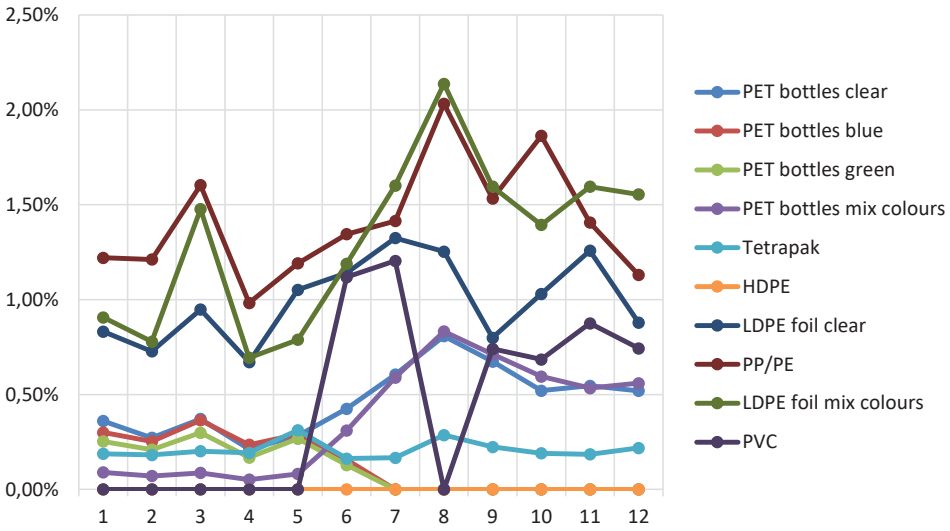

Fig. 1 Amount of sorted plastic - plant 1
Obr. 1 Množstvo vytriedených plastov - závod 1

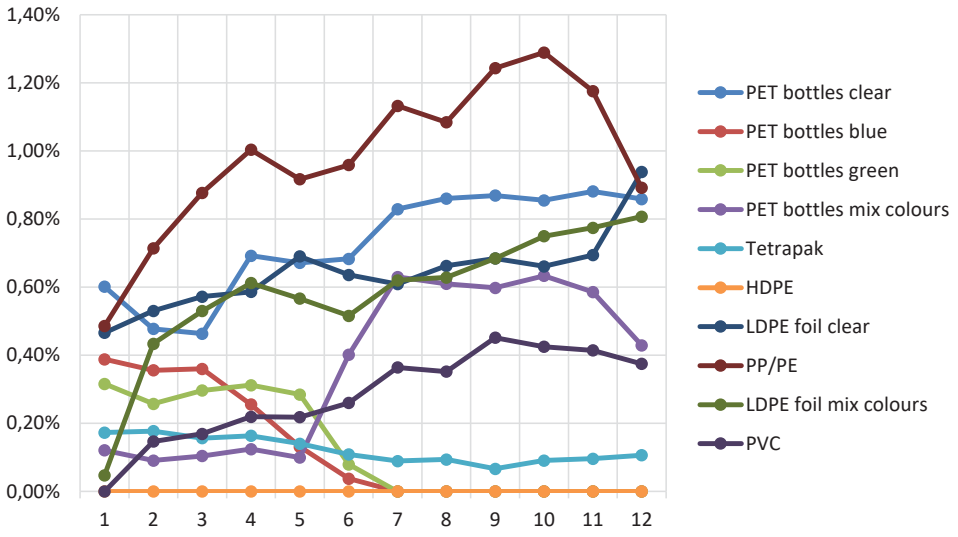

Fig. 2 Amount of sorted plastic - plant 2
Obr. 2 Množstvo vytriedených plastov - závod 2

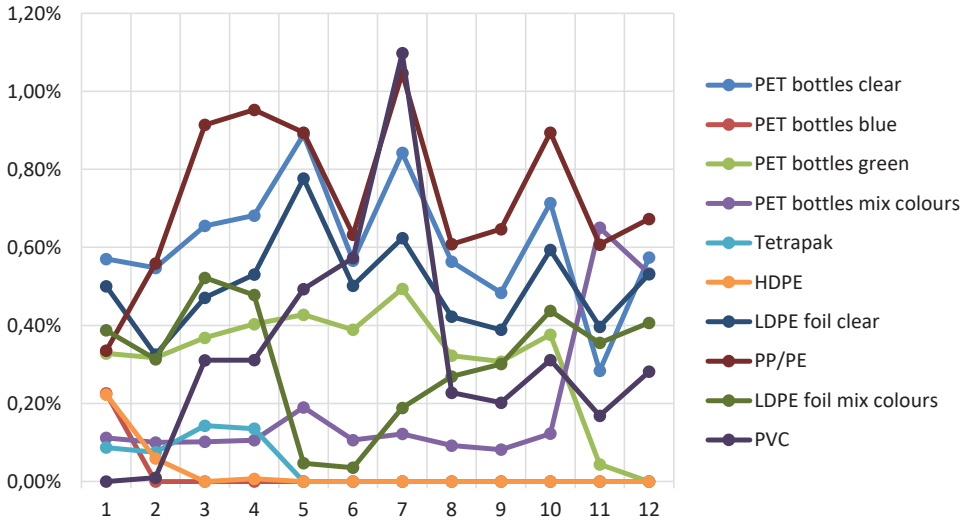

Fig. 3 Amount of sorted plastic - plant 3
Obr. 3 Množstvo vytriedených plastov - závod 3

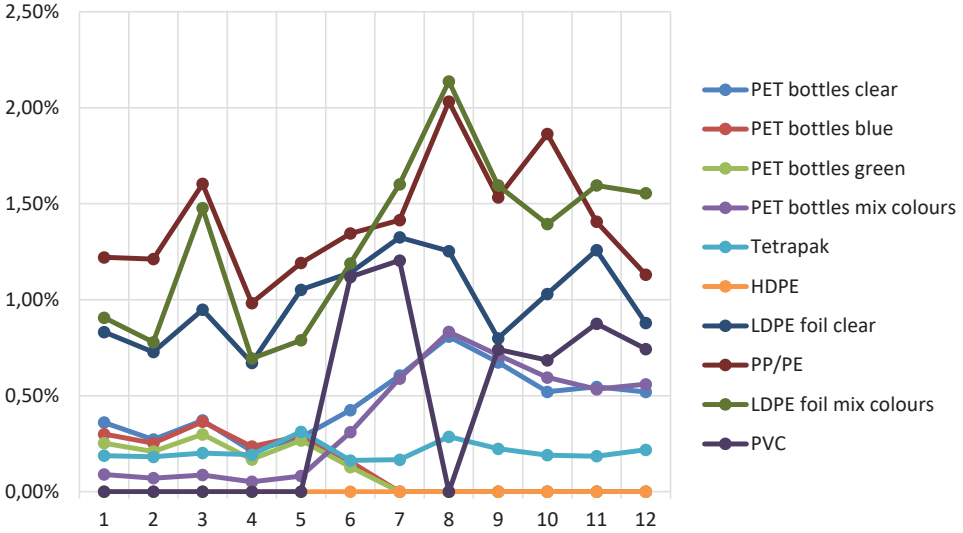

Fig. 4 Amount of sorted plastic - plant 4
Obr. 4 Množstvo vytriedených plastov - závod 4

Figs. 1 to 4 show the changing values in yields over the year. For example, the total yield of PET bottles is in plant with the higher demand in summer and at Christmas. A similar trend can be observed for LDPE films, whose production increases towards the end of the year, which can be attributed to the higher demand for packaged goods, i.e. gifts, etc. Table 3 show the results of our own analysis of mixed plastics.

Table 3 Analysis of plastic waste
Tabuľka 3 Analýza plastového odpadu

Type of commodity	**percentage of weight [%]**
PP / PE	3,00 %
LDPE clear foils	6,00 %
LDPE foils mix colours	6,00 %
PP – bottles, cups, etc.	5,00 %
HDPE bottles	3,00 %
Tetrapak	1,50 %
PET bottles clear	8,00 %
PET bottles blue and green	7,00 %
PET bottles brown, pink, red	2,00 %
PVC	2,00 %
Al metals	0,50 %
Fe metals	1,00 %
Total sortable materials	45,00 %
Not sortable materials	55,00 %

Own analysis shows that the recovery of plastics is on average 45%. On manual sorting plants, the average yield was 52,92 %. The increase compared to the actual analysis can be attributed to the better knowledge of the operators on the sorting plants, their motivation in relation to the rewards for yield and possibly also to errors, as the quality of the plastics sorted is not inherently monitored on the sorting plants, i.e. if there is no other commodity in one commodity, for example. In the actual analysis, 100 % control of the sorted plastics took place and the yield can be assessed as the maximum possible when 100 % control of the quality of the sorted plastics is observed.

DISCUSSION

Manual sorting plants are proven and affordable technologies for sorting mixed plastics. With regard to capacity, they achieve standard yields. Their biggest disadvantage is the low input capacity (*Robert et al., 2017*). Another disadvantage is the inability of humans to distinguish between different types of plastic, as e.g. spectrophotometric technologies can do. *Eriksen et al.*, (2023) state that manual sorting plants expose people to dust, endotoxin and mould particles, which have a negative impact on human health. Manual sorting plants are gradually being replaced by machine plants - automatic. These plants do not achieve higher yields, as this is not possible due to the nature of the composition of the plastics, as shown by our own analysis, see Table 3. However, they can process many times more material (*Wahab, 2006*). Lim et al., (2023) show different methods of sorting mixed plastics, through flotation, electrostatic separation to spectrophotometry. Robotic devices are more frequently used in plastics sorting (*Aschenbrenner et al., 2023*). Based on neural networks and deep learning, further improvements in plastics sorting are being made (*Pučnik et al., 2024*). Greater plant capacity also yields better economic results (*Cimpan et al., 2016*).

CONCLUSION

Sorting plastics is an important part of the plastics life cycle. Results from individual sorting plants show that manual sorting has its uses and achieves reasonable yields. However, it is safe to say that their capacity is limited. Furthermore, the results show that as the capacity of the equipment increases, their yields decrease. Manual sorting is not suitable for human health. Considering the increasing amount of waste (*Bergmann et al., 2022*), it is necessary to think about the future sorting and functionality of the whole system. Gradual automation of the sorting process, i.e. replacing manual work by machines, seems to be the solution (*Lim et al., 2023*). The most efficient manual sorting plants in the country process between 6 and 8 thousand tonnes of waste per year, with yields below 40%. The largest automatic sorting plant in the world is located in Motala, Sweden and processes up to 200 000 tonnes of plastic waste per year („World‘s Biggest Plastic Sorting Facility Inaugurated“). This plant achieves yields of up to 95% and sorts 12 types of plastics and ferrous and non-ferrous metals. As only 42% of plastics are closed loop under current conditions, the development of sorting plants and their improvement can be expected (*Eriksen et al., 2019*).

REFERENCES

ASCHENBRENNER, D., COLLOSEUS, C., KHOURY, R., FANGEROW, N. 2023. Robot-assisted automated sorting techniques for plastic recycling. Procedia CIRP, 120, 1232-1237. https://doi.org/10.1016/j.procir.2023.09.154

BERGMANN, M., COLLARD, F., FABRES, J., GABRIELSEN, G. W., PROVENCHER, J. F., ROCHMAN, C. M., VAN SEBILLE, E., TEKMAN, M. B. 2022. Plastic pollution in the Arctic. Nature Reviews Earth & Environment, 3(5), 323-337. https://doi.org/10.1038/s43017-022-00279-8

CALLEWAERT, P., LERCHE RAADAL, H., LYNG, K. -A. 2023. How to achieve ambitious recycling targets for plastic packaging waste? The environmental impact of increased waste separation and sorting in Norway. Waste Management, 171, 218-226. https://doi.org/10.1016/j.wasman.2023.08.037

CIMPAN, C., MAUL, A., WENZEL, H., PRETZ, T. 2016. Techno-economic assessment of central sorting at material recovery facilities – the case of lightweight packaging waste. Journal of Cleaner Production, 112, 4387-4397. https://doi.org/10.1016/j.jclepro.2015.09.011

DEARMITT, C. 2020. The plastics paradox: Facts for a brighter future. Phantom Plastics.

ERIKSEN, M. K., DAMGAARD, A., BOLDRIN, A., ASTRUP, T. F. 2019. Quality Assessment and Circularity Potential of Recovery Systems for Household Plastic Waste. Journal of Industrial Ecology, 23(1), 156-168. https://doi.org/10.1111/jiec.12822

ERIKSEN, E., AFANOU, A. K., MADSEN, A. M., STRAUMFORS, A., GRAFF, P. 2023. An assessment of occupational exposure to bioaerosols in automated versus manual waste sorting plants. Environmental Research, 218. https://doi.org/10.1016/j.envres.2022.115040

GADALETA, G., DE GISI, S., BINETTI, S. M. C., NOTARNICOLA, M. 2020. Outlining a comprehensive techno-economic approach to evaluate the performance of an advanced sorting plant for plastic waste recovery. Process Safety and Environmental Protection, 143, 248-261. https://doi.org/10.1016/j.psep.2020.07.008

KROELL, N., CHEN, X., KÜPPERS, B., SCHLÖGL, S., FEIL, A., GREIFF, K. 2024. Near-infrared-based quality control of plastic pre-concentrates in lightweight-packaging waste sorting plants. Resources, Conservation and Recycling, 201. https://doi.org/10.1016/j.resconrec.2023.107256

LAHTELA, V., HYVÄRINEN, M., KÄRKI, T. 2019. Composition of Plastic Fractions in Waste Streams: Toward More Efficient Recycling and Utilization. Polymers, 11(1). https://doi.org/10.3390/polym11010069

LIM, J., AHN, Y., KIM, J. 2023. Optimal sorting and recycling of plastic waste as a renewable energy resource considering economic feasibility and environmental pollution. Process Safety and Environmental Protection, 169, 685-696. https://doi.org/10.1016/j.psep.2022.11.027

MA, J., HIPEL, K. W., HANSON, M. L., CAI, X., LIU, Y. 2018. An analysis of influencing factors on municipal solid waste source-separated collection behavior in Guilin, China by Using the Theory of Planned Behavior. Sustainable Cities and Society, 37, 336-343. https://doi.org/10.1016/j.scs.2017.11.037

MINELGAITĖ, A., LIOBIKIENĖ, G. 2019. Waste problem in European Union and its influence on waste management behaviours. Science of The Total Environment, 667, 86-93. https://doi.org/10.1016/j.scitotenv.2019.02.313

NAYANATHARA THATHSARANI PILAPITIYA, P. G. C., RATNAYAKE, A. S. 2024. The world of plastic waste: A review. Cleaner Materials, 11. https://doi.org/10.1016/j.clema.2024.100220

PUČNIK, R., DOKL, M., FAN, Y. V., VUJANOVIĆ, A., NOVAK PINTARIČ, Z., AVISO, K. B., TAN, R. R., PAHOR, B., KRAVANJA, Z., ČUČEK, L. 2024. A waste separation system based on sensor technology and deep learning: A simple approach applied to a case study of plastic packaging waste. Journal of Cleaner Production, 450. https://doi.org/10.1016/j.jclepro.2024.141762

Plastic waste and recycling in the EU: facts and figures | Topics | European Parliament. (n.d.). Topics

| European Parliament. ttps://www.europarl.europa.eu/topics/en/article/20181212STO21610/plastic-waste-and-recycling-in-the-eu-facts-and-figures
Rebecca. "World's Biggest Plastic Sorting Facility Inaugurated." Smart City Sweden, 20 Nov. 2023, smartcitysweden.com/worlds-biggest-plastic-sorting-facility-inaugurated/. Accessed 26 Apr. 2024.
ROBERT, G., MARCIN, P., MAREK, M. 2017. Analysis of Picked up Fraction Changes on the Process of Manual Waste Sorting. Procedia Engineering, 178, 349-358. https://doi.org/10.1016/j.proeng.2017.01.063
ROOSEN, M., MYS, N., KUSENBERG, M., BILLEN, P., DUMOULIN, A., DEWULF, J., VAN GEEM, K. M., RAGAERT, K., DE MEESTER, S. 2020. Detailed Analysis of the Composition of Selected Plastic Packaging Waste Products and Its Implications for Mechanical and Thermochemical Recycling. Environmental Science & Technology, 54(20), 13282-13293. https://doi.org/10.1021/acs.est.0c03371
ŠŤASTNÁ, J. 2013. Všechno, co potřebujete vědět o odpadech a neměli jste se koho zeptat. EKO-KOM.
TRIPATHI, P., RAO, L. 2023. Pyrolysis and combustion kinetics of refuse derived fuel having different plastic ratio. Bioresource Technology Reports, 23. https://doi.org/10.1016/j.biteb.2023.101559
VLKOV, J. (n.d.). Automatická třídící linka na odpad pro Prahu za 100 milionů nefunguje. Spor s rakouskou firmou může skončit u soudu. Hospodářské Noviny (HN.cz). https://archiv.hn.cz/c1-67305170-automaticka-tridici-linka-na-odpad-pro-prahu-za-100-milionu-nefunguje-spor-s-rakouskou-firmou-muze-skoncit-u-soudu
WAHAB, DJURAIDAH ABDUL, et al. Development of a prototype automated sorting system for plastic recycling. American Journal of Applied Sciences, 2006, 3.7: 1924-1928.
WALKER, T. R., FEQUET, L. 2023. Current trends of unsustainable plastic production and micro(nano)plastic pollution. TrAC Trends in Analytical Chemistry, 160. https://doi.org/10.1016/j.trac.2023.116984
ZHANG, L., LIU, Y., ZHAO, Z., YANG, G., MA, S., ZHOU, C. 2023. Estimating the quantities and compositions of household plastic packaging waste in China by integrating large-sample questionnaires and lab-test methods. Resources, Conservation and Recycling, 198. https://doi.org/10.1016/j.resconrec.2023.107192

Corresponding author:
Ing. Jan Šonský, +420 737 874 607, sonskyj@tf.czu.cz

OPERATIONAL TESTING OF GASOLINE FUEL ADDITIVE IN AUTOMOBILE

PREVÁDZKOVÉ SKÚŠKY PRÍSADY DO BENZÍNU V AUTOMOBILE

Martin Krasňanský[1], Ivan Janoško[2]

[1]Institute of Agricultural Engineering, Transport and Bioenergetics, Department of Transport and Handling, Faculty of Engineering, Slovak University of Agriculture in Nitra, Tr. A. Hlinku 2, 949 76 Nitra, Slovak Republic, email: xkrasnansky@uniag.sk

[2]Institute of Agricultural Engineering, Transport and Bioenergetics, Department of Transport and Handling, Faculty of Engineering, Slovak University of Agriculture in Nitra, Tr. A. Hlinku 2, 949 76 Nitra, Slovak Republic, email: ivan.janosko@uniag.sk

ABSTRACT: The present papers deal with the issue of assessing the influence of the selected additive to automobile gasoline fuel on the power, energy and emission parameters of the selected motor vehicle Renault Clio 1,2i. Nowadays, due to the constant development in the field of automobile transport, it is necessary to carefully monitor the impact of motor vehicle operation on the environment. The main indicators in this area are vehicle consumption, which is followed by motor vehicle emissions. Fuel Save Natural 95 gasoline from Shell was used for laboratory measurement. During the entire measurement process, we used VIF Super Benzin Aditiv gasoline engine additive. Measurements of individual parameters were carried out in laboratory conditions in the form of simulated driving cycles on the cylinder test bench of motor vehicles. As an external measuring device, we used the flowmeter to measure fuel consumption. A combined exhaust gas analyzer was used to determine the representation of individual emission components in exhaust gases. The power parameters were assessed based on a comparison of the external speed characteristics of the motor vehicle. Performance of the speed characteristics of the vehicle engine was carried out twice before and after the addition of the additive. Energy and emission parameters were determined in the form of vehicle load during selected time intervals. Ten time measurements were carried out at an engine speed of 3400 min-1 with the 4th gear engaged and according to a preselected 120 second time interval. The value of unburned hydrocarbons HC decreased by 50 % and carbon monoxide CO decreased more than 30 %. For fuel consumption, we found that it increased slightly due to the increased average rpm and power. After evaluating the results, partial changes are visible in all measured parameters of the vehicle which confirms the effectiveness of tested additive with the given fuel even after a short-term use.

Keywords: additives to gasoline, gasoline, testing of automobile, consumption, emissions

ABSTRAKT: Predložený príspevok sa zaoberá problematikou hodnotenia vplyvu zvolenej prísady do automobilového benzínu na výkonové, energetické a emisné parametre vybraného motorového vozidla Renault Clio 1,2i. V dnešnej dobe vzhľadom na neustály vývoj v oblasti automobilovej

dopravy je potrebné dôsledne sledovať vplyv prevádzky motorových vozidiel na životné prostredie. Hlavnými ukazovateľmi v tejto oblasti sú spotreba vozidiel, na ktorú nadväzujú emisie motorových vozidiel. Na laboratórne meranie bol použitý benzín Fuel Save Natural 95 od značky Shell. Počas celého procesu merania sme použili aditívum do benzínových motorov VIF Super Benzin Aditiv. Merania jednotlivých parametrov boli realizované v laboratórnych podmienkach formou simulovaných jazdných cyklov na valcovej skúšobni motorových vozidiel. Ako externé meracie zariadenie sme na meranie spotreby paliva použili prietokomer. Na zistenie zastúpenia jednotlivých emisných zložiek vo výfukových plynoch bol použitý päťplynový kombinovaný analyzátor výfukových plynov. Výkonové parametre boli hodnotené na základe porovnania vonkajších otáčkových charakteristík motorového vozidla. Vykonávanie otáčkových charakteristík motora vozidla bolo realizované dvakrát pred a po pridaní aditíva. Energetické a emisné parametre boli zisťované formou zaťaženia vozidla počas zvolených časových intervalov. Vykonalo sa desať časových meraní z toho 5 pred pridaním aditíva a 5 po pridaní aditíva pri otáčkach motora 3400 min-1 so zaradeným 4. prevodovým stupňom a podľa vopred zvoleného 120 sekundového časového intervalu. Meranie s aditívom ukázalo, že hodnota nespálených uhľovodíkov HC klesla asi o 50 % a oxidu uhoľnatého CO sa znížil o viac ako 30 %. Vyhodnotené výsledky ukazujú čiastkové zmeny vo všetkých nameraných parametroch vozidla, čo potvrdzuje účinnosť testovaného aditíva s daným palivom aj po krátkodobom používaní. Pri spotrebe paliva sme zistili, že sa mierne zvýšila v dôsledku zvýšených priemerných otáčok a výkonu.

Kľúčové slová: prísady do benzínu, benzín, testovanie automobilu, spotreba, emisie

INTRODUCTION

Today, due to the constant development in the field of automobile transport, it is necessary to closely monitor the influence and impact of the operation of motor vehicles on the living environment. Today, due to the constant development in the field of automobile transport, it is necessary to closely monitor the influence and impact of the operation of motor vehicles on the living environment. The main indicators in this area are vehicle consumption, which is subsequently followed by motor vehicle emissions (*Gondžár, 1990; Vlk, 2006*). Various types of fuel are used in vehicles, with gasoline being one of the most common. Automotive gasoline is a mixture of liquid hydrocarbons with a boiling point in the temperature range from 30 °C to 210 °C. The basic requirements for gasoline are a good evaporation at low temperatures, a low content of sulfur, which causes corrosion of the fuel system, the absence of heavy fractions and resin, which causes clogging of nozzles, intake pipe and valves (*Semetko, 1996; Jablonický, 2010; Králik et al. 2016; Synák F., Synák, J., 2022*). The most important harmful substances in exhaust gases are carbon monoxide CO, unburned hydrocarbons HC and nitrogen oxides NOx. As the ignition advance increases, NOx emissions and subsequently also HC emissions increase. CO emissions are almost independent of ignition advance and are almost exclusively a function of the excess air factor. Adding the additive to a gasoline has recently become a more and more discussed topic. Various preparations in the form of additive concentrates are added to gasoline. These preparations are intended for addition directly to the fuel tank during refueling or before refueling to ensure the most perfect mixing of the additive with the fuel due to the flow of fuel entering the tank. These are substances acting to increase resistance to detonation combustion, reduce fuel consumption, purify the fuel and intake tract, reduce engine friction and subsequently increase its power, etc. (*Matějovský, 2005; Vlk, 2006; Hromádko, 2011; Lenďák, Jablonický, 2015; Sarkan et al., 2017*; STN EN

228 + A1: 2018; Slovak Republic Decree no. 251/2023 Coll.). The measurements will be aimed at achieving the best possible results when measuring consumption, emissions and other parameters of the selected motor vehicle in laboratory conditions on the cylinder test bench.

MATERIAL AND METHODS

Characteristic of used material

A Renault Clio passenger car belonging to the M1 category was used for the measurement. The technical parameters of the vehicle can be found in Tab. 1. During the entire measurement process, Matador MP 56 winter tires with size 175/65 R14 were used and inflated to the prescribed operating pressure of 200 kPa. Fuel Save Natural 95 from Shell brand was used for laboratory measurement of fuel consumption and emissions. It is 95 octan unleaded gasoline. There were approximately 25 liters of gasoline in the tank during the test. During the entire measurement process, we used the additive for gasoline engines VIF Super Benzin Aditiv, which was used in the ratio of 125 ml of additive to 25 litres of fuel. The total resulting mixing ratio after adding the additive in the tank reached a value of 1:200. The additive is intended for all spark-ignition engines with direct and indirect fuel injection. The manufacturer declares a reduction in fuel consumption by an average of 5-7%, a reduction in friction in the engine and thus an increase in performance, maintaining the cleanliness of the fuel system, improving the cold start of the engine, preserving the full function and life of catalysts and protection against corrosion. The additive contains kerosene CAS 64742-81-0, aromatic fraction CAS 64742-94-5.

Fig. 1 Tested vehicle Renault Clio 1,2i
Obr. 1 Testovaný automobil Renault Clio 1,2i

Table 1 Parameters of used automobile Renault Cio 1,2i
Tabuľka 1 Parametre použitého automobilu Renault Clio 1,2i

Automobile Renault Clio 1,2i	
Type[1)]	Passenger car
Category[2)]	M1
Motor (type)[3)]	D7FG7
Engine capacity[4)] [cm^3]	1149
Maximum engine power [kW] / rpm[5)] [min^{-1}]	43 / 5250
Overall dimensions length – width – height[6)] [mm]	3773 – 1639 – 1417
Operational weight[7)] [kg]	945
Maximum permissible total weight[8)] [kg]	1445

[1)]Typ, [2)]Kategória, [3)]Motor (typ), [4)]Objem motora, [5)] Maximálny výkon/otáčky,[6)]Celkové rozmery vozidla [7)]Prevádzková hmotnosť, [8)]Maximálna povolená celková hmotnosť

Characteristic of used devices

The first and most basic device will be the MSR 500 ALLRAD (4W) cylinder test unit from the manufacturer Maschinenbau Haldenwang (MAHA) enabling testing of 4x4 vehicles.

Fig. 2 Cylinder test unit MAHA MSR 500
Obr. 2 Valcová výkonová skúšobňa MAHA MSR 500

An AIC - 5004 FUEL FLOWMASTER from AIC SYSTEMS AG was used as an external measuring device to measure fuel consumption. To determine the representation of individual emission components in exhaust gases, a five-gas combined non-dispersive infrared NDIR exhaust gas analyzer of the brand MAHA Kombi tester MGT/MDO2 – LON for spark-ignition and diesel engines was used, consisting of both analysis stations in cooperation with a personal computer with MAHA Emission Software for measurement and evaluation of measured data. A MAHA Air 7 radial fan with an ACA 132M - 4 electric motor with a power of P = 7.5 kW, maximum rpm = 1440 min^{-1} and efficiency n = 86 % was used to cool the engine of the test car (Maha, 2024; Maha Emission Tester, 2024; Seka, 2024).

Characteristics of work procedures

The measurement methodology consists of the following sub-tasks:

- Fixing the vehicle in accordance with the prescribed standards,
- Connecting the flow meter to the fuel system of the vehicle,
- Insert of an oil temperature sensor instead of an engine oil dipstick,
- Checking for leaks and connecting the exhaust gas analyzer to the vehicle's exhaust system,
- Pairing of measuring stations (emission station and cylindrical test bench measuring station) via LAN network
- Pairing of the vehicle with measuring stations via on-board diagnostics

The measurement procedure

- Preparing the vehicle for measurement according to the instructions in the measurement methodology
- Heating up motor of vehicle to operating temperature
- Performing of engine speed characteristics of vehicle's engine twice before and after adding the additive
- Carrying out ten time measurements, of which 5 before the addition of the additive and 5 after the addition of the additive by starting the car to a speed corresponding to the engine speed of 3400 min^{-1} with the 4th gear engaged and according to a pre-selected 120 second time interval of driving simulation during the vehicle reached the required conditions, those were constantly maintained throughout the measured section and during which the data were recorded
- Among the most important emission values, we included the values of unburned HC and CO while the emission limits that the vehicle must meet are as follows: CO 2.30 $g.km^{-1}$; HC 0.20 $g.km^{-1}$ and parameter of fuel consumption of 6.0 $l.100\ km^{-1}$.
- Adding the additive to the fuel, choosing a 30-minute simulation period during which the additive was mixed with the fuel based on a certain engine load with a constant pulling force of 150 N, and re-taking the time and power measurements.
- Saving measurement results, their analysis and conclusion, subsequent export of all measurement results to a memory medium.

It was necessary to calculate and analyse measured parameters using the basic following relationships:

Calculation of performance

$$P = M_k.\omega = M_k.2.\pi.n \quad [\text{kW}] \tag{1}$$

where: P is performance [kW]
M_k is torque [Nm]
ω is angular speed
n are revolutions [min^{-1}]

Calculation of torque

$$M_k = \frac{P}{2.\pi.n} \quad [\text{Nm}] \tag{2}$$

The quantity of fuel consumed for the selected period of time

$$V' = V_{x1} - V_{x2} \quad [\text{dm}^3.(30\text{s}^{-1})] \tag{3}$$

V' is quantity of fuel consumed for the selected period of time [dm^3.(30 s^{-1})]
V_{x1} is volume of fuel in the tank at time t_1
V_{x2} is volume of fuel in the tank at time t_2

Hourly fuel consumption

$$V = \frac{V'.\rho_f}{t}.3600 \quad [\text{kg.hod}^{-1}] \tag{4}$$

where: V is fuel consumption for 1 hour [kg.hod^{-1}]
ρ_f is density of fuel [kg.m^{-3}]
t is time [h]

RESULTS

All measurements were performed in pre-agreed time intervals and number of measurements to achieve the best possible results. When driving on a cylindrical test bench, a constant tensile force of 500 N was specified for all measurements. From the point of view of consumption, the decisive measured data is the volume of injected fuel V given in litres. Figure 1 shows the time dependence curves of the measured data of one of the five measurements before adding the additive, and Figure 2 shows the time dependence curves of the measured data of one of the five measurements after the addition of the additive. Then an average value was made from all five measurements. The values of unburned HC decreased by an average of 4.92 ppm by volume and a difference of 0.03 % by volume of CO before and additive addition was found out. In terms of fuel consumption, there was found an increase of 0.319 kg.hod^{-1}, which is basically a real value due to the increased average rpm and increased average power in the measurements after addition of additive to the fuel compared to the values before addition of the additive to the fuel.

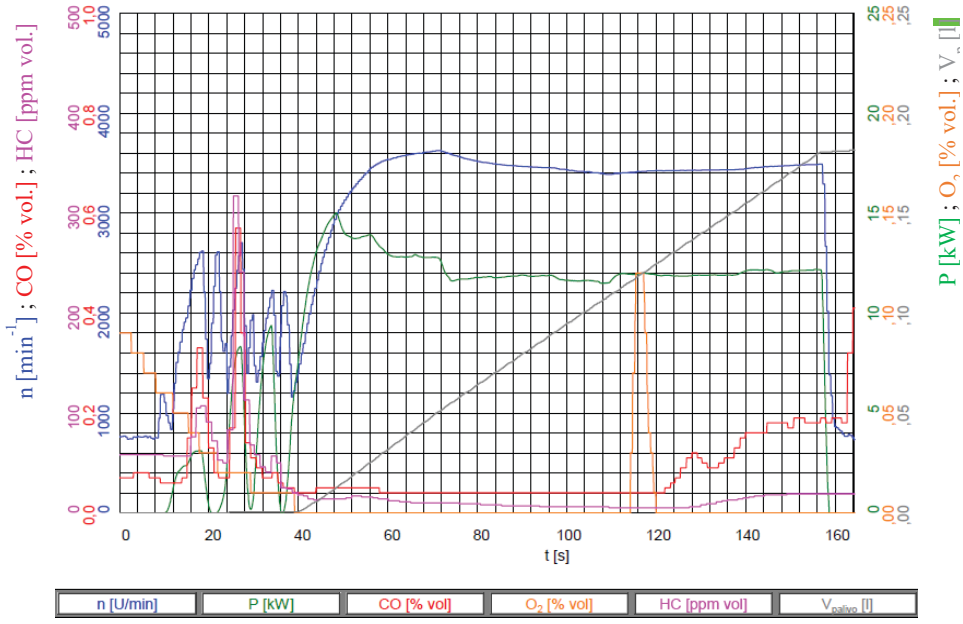

Fig. 1 Time dependence of measured data (n – revolutions [min-1], P – engine power [kW], CO – Carbon monoxide [% vol.], O2 – Oxygen [% vol.], HC – Unburned hydrocarbons [ppm vol.], V – fuel volume [l]) without additive

Obr. 1 Časová závislosť nameraných údajov (n – otáčky motora [min^{-1}], P – výkon motora [kW], CO – oxid uhoľnatý [obj. %], O_2 – kyslík [obj. %], HC – nespálené uhľovodíky [ppm obj.], V – objem paliva [l]) bez aditíva

Based on the evaluation, it can be determined that after adding the additive, the engine power parameter improved by 3.3 kW. The power loss was increased by 1.6 kW, which is a value indicating total losses resulting from the sum of power losses, which include losses in wheels, differentials, bearings, etc. Fig. 3 shows speed characteristic without additive and Fig. 4 shows speed characteristic with added additive. In Table 2 can be seen the results of measuring emissions, fuel consumption, revolutions and engine power before and after adding additive together with standard deviation and variation coefficient and in Tab. 3 can be seen differences in speed characteristics before and after addition of additive.

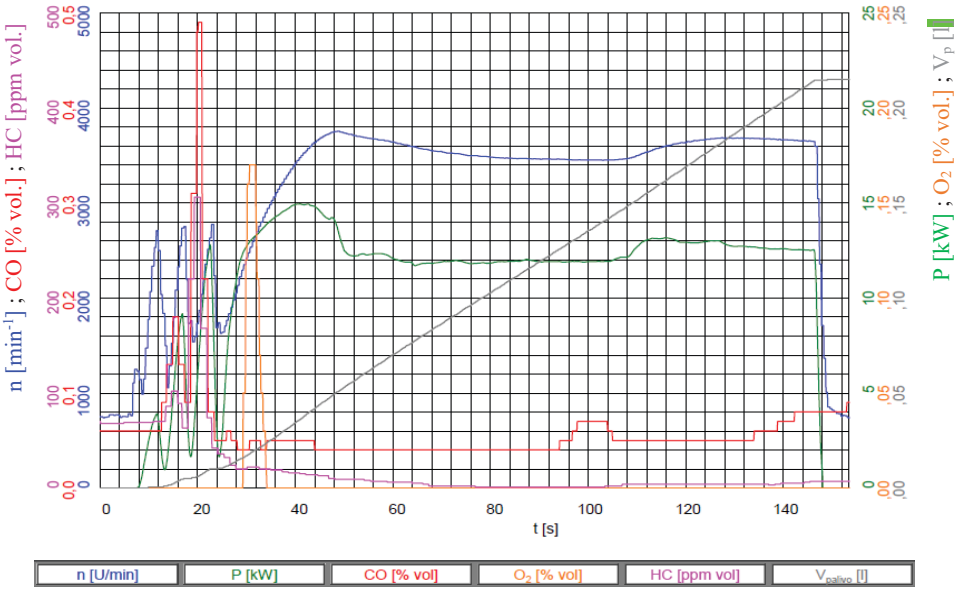

Fig. 2 Time dependence of measured data (n – revolutions [min^{-1}], P – engine power [kW], CO – Carbon monoxide [% vol.], O_2 – Oxygen [% vol.], HC – Unburned hydrocarbons [ppm vol.], V – fuel volume [l]) with additive

Obr. 2 Časová závislosť nameraných údajov (n – otáčky motora [min^{-1}], P – výkon motora [kW], CO – oxid uhoľnatý [obj. %], O_2 – kyslík [obj. %], HC – nespálené uhľovodíky [ppm obj.], V – objem paliva [l]) s aditívom

Table 2 Results of measuring emissions, fuel consumption, revolutions and engine power before and after adding additive together with standard deviation and variation coefficient

Tabuľka 2 Výsledky meraní emisií, spotreby paliva, otáčok motora a výkonu motora pred a po pridaní aditíva do paliva spolu so smerodajnou odchýlkou a variačným koeficientom

Automobile Renault Clio	Time of measurement	Average values	Standard deviation	Variation coefficient
Revolutions n[1)] (min^{-1})	before addition	3467	73,49	0,021
	after addition	3533	57,90	0,016
Engine power P[2)] (kW)	before addition	11,97	0,29	0,024
	after addition	12,20	0,29	0,023
Carbon monoxide CO[3)] (% of vol.)	before addition	0.083	0.025	0.303
	after addition	0.050	0.043	0.860
Unburned hydrocarbons HC[4)] (ppm vol.)	before addition	9,660	5,650	0.585
	after addition	4.740	7,860	1.658
Fuel consumption[5)] (kg. hod^{-1})	before addition	4,324	0.182	0.042
	after addition	4,643	0.075	0.016

[1)]Otáčky za minútu, [2)]Výkon motora, [3)]Oxid uhoľnatý, [4)]Nespálené uhľovodíky, [5)]Spotreba paliva

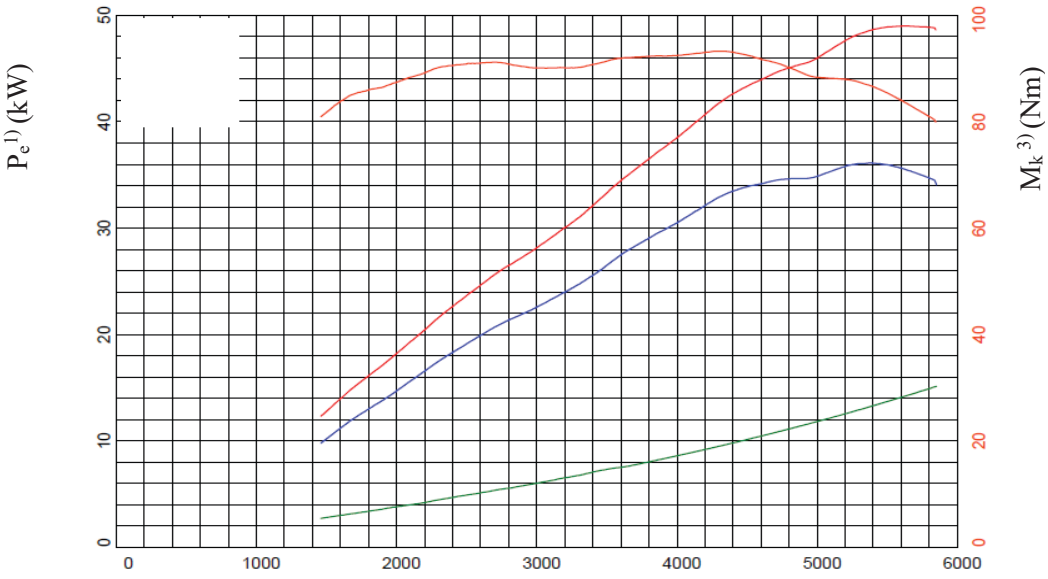

Fig. 3 Speed characteristic without additive
Obr. 3 Otáčková charakteristika bez pridaného aditíva
[1] Effective performance, [2] Revolutions per minute, [3] Torque
Standardized torque M_{norm} [Nm], Standardized performance P_{norm} [kW]
Lossy performance P_s [kW], Performance on wheels P_k [kW]
[1] Efektívny výkon, [2] Otáčky za minútu, [3] Krútiaci moment
Normovaný krútiaci moment M_{norm} [Nm], Normovaný výkon P_{norm} [kW],
Stratový výkon P_s [kW], Výkon na kolesách P_k [kW]

Table 3 Differences in values of speed characteristics before and after adding additive
Tabuľka 3 Rozdiely v hodnotách otáčkových charakteristík pred a po pridaní aditíva

Comparison of power parameters of speed characteristics		
Parameter	**Before adding additive**	**After adding additive**
Engine power P_{mot} [1] [kW]	47,1	50,4
Maximum power at rpm [min^{-1}] / speed [2] [$km.h^{-1}$]	5460 / 137	5735 / 143,7
Torque M_k [3] [Nm]	93,2	94,3
Maximum torque at revolutions [min^{-1}] / speed [4] [$km.h^{-1}$]	3695 / 92,7	4195 / 105,1
Maximum revolutions [min^{-1}] / speed [5] [$km.h^{-1}$]	6105 / 153,3	6135 / 153,8

[1]Výkon motora, [2]Maximálny výkon pri otáčkach / rýchlosti, [3]Krútiaci moment, [4]Maximálny krútiaci moment pri otáčkach / rýchlosti, [5]Maximálne otáčky / pri rýchlosti

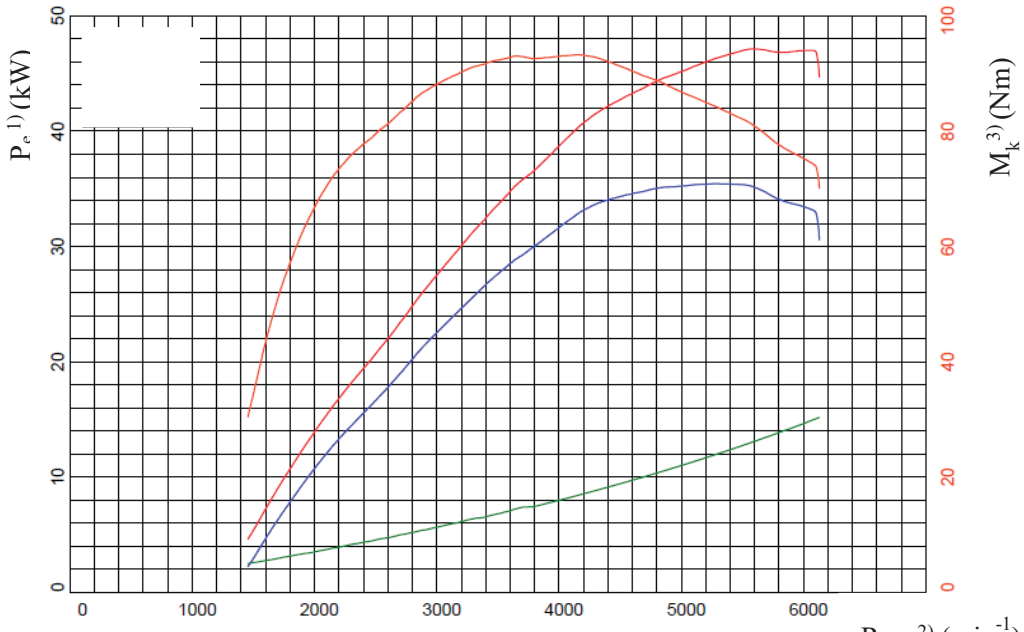

Fig. 4 Speed characteristic with additive
Obr. 4 Otáčková charakteristika s pridaným aditívom
[1)] Effective performance, [2)] Revolutions per minute, [3)] Torque
Standardized torque M_{norm} [Nm], Standardized performance P_{norm} [kW]
Lossy performance P_s [kW], Performance on wheels P_k [kW]
[1)] Efektívny výkon, [2)] Otáčky za minútu, [3)] Krútiaci moment
Normovaný krútiaci moment M_{norm} [Nm], Normovaný výkon P_{norm} [kW],
Stratový výkon P_s [kW], Výkon na kolesách P_k [kW]

DISCUSSION

Similar research was carried out by Masyaroh et al. (2024) who researched the physicochemical properties of limonene and eugenol additives in n-heptane and low-octane gasoline to evaluate their effects on the emission characteristics and fuel consumption of single-cylinder gasoline engines. The addition of eugenol reduced CO and HC emissions compared with limonene, which only decreased HC emissions. Xiaoteng et al. (2023) firstly studied the effects of eleven unconventional additives including alcohol, ether, amine, esters, and phenolic on the physicochemical properties of commercially available 92# and 95# gasoline and then the economic performance, emission performance, and acceleration performance of passenger vehicle equipped with PFI engine fueled with different additives were studied by drum test simulating real road driving conditions. Behcet, Yakin (2022) tested three different fuel types in a single-cylinder gasoline engine. The aim of this study was to obtain alternative fuels with hydrogen-containing ($NaBH_4$) and oxygen-containing (ethanol, methanol) fuel additives and to test these fuels in a gasoline engine. For this purpose, each of the $NaBH_4$ added ethanol and methanol solutions was added to pure gasoline at a volume of 10% and mixed fuels named SE10 and SM10 were obtained

and found out that adding $NaBH_4$ doped ethanol and methanol solutions to pure gasoline resulted in better combustion, reductions in CO emissions of SE10 and SM10 blended fuels by 31.04 % and 53.7 %, but CO_2 emissions increased by 11.20 % and 19.51 % respectively. In addition, NO_x emissions of SE10 and SM10 blended fuels decreased by 15.17 % and 8.73 %, respectively. The authors Janoško, Feriancová (2019) assessed the impact of the VIF additive used in diesel fuel on improving the power and emission parameters of the vehicle and its consumption. The results of the experimental measurements of these authors partially show the positive influence of the selected additive on the fuel consumption and emissions of the tested passenger car. Measurements on the vehicle showed that NOx emissions decreased by 4 %, but fuel consumption increased by 1 %. The author Podskalan (2021) carried out similar research, where he tested the same VIF additive on a Škoda 100 vehicle, while the author came to the same conclusion that with the help of the fuel additive he managed to reduce NOx emissions by 11.71 % and when measuring fuel consumption, he recorded a reduction of 5,44 % after adding the VIF additive.

CONCLUSION

- The aim of the research was to assess the influence of the selected additive to automotive gasoline on the performance, energy and emission parameters of the selected automotive vehicle.
- The object of the research was a Renault Clio 1,2i automobile with an atmospheric engine with a volume of 1.2 l and the maximum engine power of 43 kW.
- The difference was visible in all measured vehicle parameters.
- Due to the effect of fuel additive, a partial difference was achieved in the parameters of the tested motor vehicle while maintaining the same measurement conditions, which confirms the effectiveness of fuel additive with the given fuel even after short-term use.
- The value of unburned HC decreased by an average value of 4.92 ppm by volume, which is a decrease in the value of unburned hydrocarbons by about more than 50 %.
- CO decreased by a value of about 0.03 % of the volume, which means that a reduction of more than 30 % was achieved from the original value before the addition of the additive.
- For fuel consumption, we found that it increased slightly due to the increased average rpm and power after the addition of additive to the fuel compared to those values before the addition of additive to the fuel.
- The overall impact of the additive on the power, energy and emission parameters of the tested vehicle after analysis is evaluated as positive.

REFERENCES

BEHCET, R., YAKIN, A. 2022. Evaluation of hydrogen-containing $NaBH_4$ and oxygen-containing alcohols (CH_3OH, C_2H_5OH) as fuel additives in a gasoline engine. *International journal of hydrogen energy*, vol. 47, no. 53, pp. 22316-22327. ISSN 0360-3199

GONDŽÁR, A., GONDŽÁR, K. 1990. *Automobily a spotreba paliva*. Praha: Nakladateľstvo dopravy a spojov. s. 284. ISBN 80-7030-085-X

HROMÁDKO, J. 2011. *Spalovací motory: komplexní přehled problematiky pro všechny typy technických automobilních* škol. Praha: Grada. ISBN 978-80-247-3475-0
JABLONICKÝ, J. 2010. *Motorové vozidlá 1*. Nitra: Slovenská poľnohospodárska univerzita. s. 97. ISBN 978-80-552-0474-1
JANOŠKO, I., FERIANCOVÁ, F. 2019. The effect of diesel additive on emissions and engine performance. In *Proceeding of 7th international conference on trends in agricultural engineering* (TAE), Prague: Czech Republic, pp.225-230. ISBN 978-80-213-2953-9
KRÁLIK, M., JABLONICKÝ, J., TKÁČ, Z., HUJO, Ľ., UHRINOVÁ, D., KOSIBA, J. et al. 2016. Monitoring of selected emissions of internal combustion engine. *Research in agriculture engineering*, vol. 62, no. 1, pp 66–70. doi: 10.17221/72/2015-RAE.
LENĎÁK, P., JABLONICKÝ J. 2015. *Návrh metodiky výkonu emisných kontrol pre vozidlá so zážihovým motorom a zdokonaleným emisným systémom.* Nitra: Slovenská poľnohospodárska univerzita. s. 208. ISBN 978-80-552-1319-4
Maha. 2024. *MSR 500 4WD*. Available from: https://www.maha.de/en/products/performance-measurement-technology/dynamometers/msr-5002-pkw-allrad~p2012
Maha Emission Tester. 2024. *MCT Maha Combi Tester*. Available from: https://www.maha.de/en/products/emission-measurement-technology/emission-tester/mct~p25150
MATĚJOVSKÝ, V. 2005. *Automobilová paliva.* Praha: Grada. S. 228. ISBN 80-247-0350-5
MUSYAROH, WIJAYANTI, W., SASONGKO, M. N., WINARTO. 2024. The effects of limonene and eugenol additives in n-heptane and low-octane gasoline on the emission characteristics and fuel consumption of single-cylinder gasoline engine. *Engineering Science and Technology, an International Journal*, vol. 51. ISSN 2215-0986
PODSKALAN, J. 2023. Hodnotenie parametrov aditíva do benzínu vyrábaného pre automobilový priemysel. Bakalárska práca. Nitra: Slovenská poľnohospodárska univerzita, Technická fakulta. s. 52. Dostupné na: https://opac.crzp.sk/?fn=detailBiblioFormChildI10FRH&sid=9CB04A0EB3E2DA9145908A0E204E&seo=CRZP-detail-kniha
SARKAN, B., STOPKA, O., GNAP, J., CABAN, J. 2017. Investigation of Exhaust Emissions of Vehicles with the Spark Ignition Engine within Emission Control. Procedia Engineering, vol. 187, 775-782 pp. DOI: 10.1016/j.proeng.2017.04.437. ISSN 18777058.
Seka. 2024. *Emission control procedure*. Available from: https://www.seka.sk/verejnost/informacie/postup-pri-emisnej-kontrole
SEMETKO, J. 1996. Vlastnosti motorových vozidiel. Nitra: Slovenská poľnohospodárska univerzita. s. 103. ISBN 80-7137-268-4
Zákon Slovenskej republiky č. 106/2018 Z. z. o prevádzke vozidiel v premávke na pozemných komunikáciách a o zmene a doplnení niektorých zákonov
Vyhláška Slovenskej republiky č. 251/2023 Z.z. o kvalite paliva
STN EN 228 + A1: 2018. Automobilové palivá. Bezolovnatý benzín. Požiadavky a skúšobné metódy.
SYNÁK, F., SYNÁK, J. 2022. Study of the impact of malfunctions of and interferences in the exhaust gas recirculation system on selected vehicle characteristics. *SAE International Journal of Engines*, vol. 15, no. 6. DOI: 10.4271/03-15-06-0041. ISSN 19463936
VLK, F. 2006. *Paliva a maziva motorových vozidel*. Brno: František Vlk. ISBN 80-239-6461-5
XIAOTENG, Z., SHOUZHEN, Z., YANG, Z., JIA, L., XIANG EN, K., SHIHAI, Z. et al. 2023. Effects of different additives on physicochemical properties of gasoline and vehicle performance. *Fuel Processing Technology*, vol. 242. ISSN 0378-3820

Corresponding author:
Martin Krasňanský, tel. +421917566904, e-mail: xkrasnansky@uniag.sk

POTENTIAL OF MAIZE BIOPHYSICAL PARAMETERS DETECTION USING SAR IMAGES

POTENCIÁL ZJIŠŤOVÁNÍ BIOFYZIKÁLNÍCH PARAMETRŮ KUKUŘICE POMOCÍ SAR SNÍMKŮ

Miloš Láznička[1], Jitka Kumhálová[2], František Kumhála[3]

[1] Czech University of Life Sciences Prague, Kamýcká 129, 16500 Prague, Czech Republic, e-mail: laznickam@tf.czu.cz
[2] Czech University of Life Sciences Prague, Kamýcká 129, 16500 Prague, Czech Republic, e-mail: kumhalova@tf.czu.cz
[3] Czech University of Life Sciences Prague, Kamýcká 129, 16500 Prague, Czech Republic, e-mail: kumhala@tf.czu.cz

ABSTRACT: The integration of Synthetic Aperture Radar (SAR) with its Radar Vegetation Index (RVI) alongside ground reference data offers a potent methodology for environmental monitoring, particularly in the field of agriculture and precision farming. This study, conducted in April 2023 in the Czech Republic, focused on a maize field provided by the Agricultural Co-operative Dolní Újezd. Leveraging SAR data sourced from Sentinel-1, a satellite mission managed by the European Space Agency (ESA), we assessed the utility of SAR imagery for delineating vegetation variability. The SAR data were processed, including resampling at varying pixel resolutions (10, 50, and 100 meters) and subsequent speckle filtering employing methodologies such as Frost, Gamma Map, Lee Sigma, Median, Refined Lee, and Boxcar. Terrain correction via Range-Doppler Terrain Correction was implemented to mitigate distortions. The computation of the RVI index, formulated as (4sigmaVH)/(sigma*VV+sigmaVH), facilitated the assessment of vegetation characteristics. Subsequent statistical analyses were performed to validate the outcomes. From the correlation analysis, it was determined that utilizing Cubic Convolution and resampling to a 10-meter resolution supplied the most consistent results with the field measurements. When it comes to fresh weight samples and plant height. However, for Ncrop measurements, Bilinear Interpolation delivered better outcomes. This investigation offered findings demonstrating a positive correlation between SAR-derived metrics and ground reference data, encompassing parameters such as plant height, fresh weight, and Ncrop measurements.

Keywords: Geoinformation, SAR, statistical analysis, speckle filtering, field variability, maize

ABSTRAKT: Spojení radaru se syntetickou aperturou (SAR) a jeho radarového vegetačního indexu (RVI) s pozemními referenčními daty, nabízí účinnou koncepci monitorování životního prostředí, zejména v oblasti zemědělství a precizního zemědělství. Tato studie, provedená v dubnu 2023 v České republice, se zaměřila na kukuřičné pole poskytnuté Zemědělským družstvem Dolní Újezd. S využitím dat SAR pocházejících z družicové mise Sentinel-1, kterou řídí Evropská kosmická agentura (ESA), byla zkoumána vhodnost použití snímků SAR pro vymezení variability vegetace. Data SAR byla podrobena zpracování, včetně převzorkování s různým rozlišením pixelů (10, 50 a 100 metrů)

a následného filtrování speckle pomocí filtrů Frost, Gamma Map, Lee Sigma, Median, Refined Lee a Boxcar. Pro zmírnění zkreslení byla provedena korekce terénu pomocí Range-Doppler Terrain Correction. Výpočet indexu RVI, formulovaný jako (4sigmaVH)/(sigma*VV+sigmaVH), usnadnil hodnocení charakteristik vegetace. K ověření výsledků byly provedeny následné statistické analýzy. Na základě korelační analýzy bylo zjištěno, že použití kubické konvoluce a převzorkování na rozlišení 10 metrů přineslo nejkonzistentnější výsledky s terénními měřeními. Pokud jde o vzorky čerstvé hmotnosti a výšky rostlin. Nicméně v případě měření Ncrop poskytla Bilineární interpolace lepší výsledky. Výzkum přinesl zjištění, která prokázala pozitivní korelaci mezi ukazateli odvozenými ze SAR a referenčními pozemními údaji zahrnujícími parametry, jako je výška rostlin, čerstvá hmotnost a měření Ncrop.

Klíčová slova: Geoinformatika, SAR, statistická analýza, speckle filtering, variabilita pole, kukuřice

INTRODUCTION

Maize (Zea mays) is a major cereal crop with significant global agricultural importance due to its high yield potential and versatility in various uses, including food, feed, and biofuel production. In agriculture, maize cultivation is critical for food security and economic stability in many regions, necessitating effective crop monitoring and management practices (El-Jubouri et. al., 2012).

In 2022, maize covered an area of 80,175 hectares, with an average yield of 7.81 tons per hectare from 2018 to 2022 (Czech Statistical Office, 2022).

Monitoring maize growth and health is essential for optimizing yield and resource use. Advanced techniques, such as remote sensing and vegetation indices, are increasingly employed to assess crop conditions, detect stress factors, and predict yield outcomes. These methods provide valuable insights into maize growth patterns, nutrient requirements, and environmental interactions, contributing to more efficient and sustainable agricultural practices. Understanding and improving maize crop management through these technologies can enhance productivity and resilience in the face of evolving environmental challenges (Stoicea, P, et al., 2023).

The integration of Synthetic Aperture Radar (SAR) technology with ground reference data holds significant promise for advancing environmental monitoring practices, particularly in agricultural contexts. This paper explores the synergistic potential of SAR imagery, Radar Vegetation Index (RVI), and field-acquired data for mapping vegetation variability, focusing on maize cultivation as a case study (Oliver, 1991), (Chris Oliver, 1998).

In this framework, the European Space Agency's (ESA) Sentinel Application Platform (SNAP) and the Quantum Geographic Information System (QGIS) are key tools. SNAP is specifically designed for processing and analyzing data from Sentinel satellite missions. It provides a range of functions for the preprocessing, visualization, and interpretation of SAR and optical data. Its modular structure allows users to incorporate additional plugins, making it a flexible tool for various remote sensing applications.

QGIS, an open-source geographic information system, supports the management and analysis of geospatial data. It enables users to view, edit, and analyze spatial data across different formats. The ability to extend QGIS's functionality through plugins enhances its utility for complex spatial analyses. Integration of QGIS with SNAP facilitates a stream-

lined workflow for processing and analyzing satellite data, supporting detailed environmental assessments.

The study by (Khabbazan et al., 2019), illustrates the efficacy of Sentinel-1 radar imagery for monitoring critical crops such as sugar beet, potato, maize, wheat, and English rye grass in the Netherlands. As the authors state, low-frequency radar is suitable for detecting soil moisture, water content, and structural variations in agricultural crops.

Speckle filters

Speckle filtering is crucial for reducing noise – speckle. It arises from coherent summation of signals scattered by randomly distributed ground scatterers within each pixel (*Davis & Jain, 2019*). Speckles reduce readability, complicating the accurate analysis of the imagery. By applying speckle filtering the image has enhanced clarity and enables more precise extraction of information.

To reduce appearance of speckles, speckle filtering applies a smoothing effect by calculating a new value for each pixel based on the surrounding pixels within a kernel. A kernel is a twodimensional grid of various size dependent on the filter. The kernel moves across the image one pixel at a time, replacing the central pixel with the calculated value until the entire image is processed (*Mansourpour et al., 2006*), (*Kulkarni & Rege, 2020*), (*Nicolas et al., 2001*).

Frost

The Frost filter replaces the pixel of interest with a weighted sum of the values in an *nxn* moving kernel. Weighting factors decrease with distance from the central pixel but increase for central pixels if variance within the kernel is higher. This filter assumes multiplicative noise with stationary statistics and follows a specific formula (Lopes et al., 1990).

$$DN = \sum_{n \times n} k \alpha e^{-\alpha |t|} \tag{1}$$

where $\alpha = (4 / n\bar{\sigma}^2)(\sigma^2 / \bar{I}^2)$

k = normalization constant

$\bar{I}$ = local mean

σ =local variance

$\bar{\sigma}$ = image coefficient of variation value

$|t| = |X\text{-}X_0| + |Y\text{-}Y_0|$, and

n = moving kernel size (Lopes et al., 1990).

Gamma Map

The Maximum A Posteriori (MAP) filter operates on a multiplicative noise model with variable mean and variance. It assumes the original DN value is between the DN of the pixel of interest and the average DN of the moving kernel. The algorithm works with natural vegetated areas modeled with a Gamma distribution (Frost et al., 1982).

$$\bar{I}^3 - \bar{I}\hat{I}^2 + \sigma(\hat{I} - DN) = 0 \tag{2}$$

where $\bar{I}$ = sought value
$\bar{I}$ = local mean
DN = input value
σ = the original image variance.

Lee Sigma and Lee

The Lee-Sigma and Lee filters estimate the value of a pixel by using the statistical distribution of digital number (DN) values within a moving kernel. Both filters assume that the noise in the image data follows a Gaussian distribution. The Lee filter specifically operates on the assumption that the mean and variance of the pixel of interest match the local mean and variance of all pixels within the chosen kernel. The formula for the Lee filter is (*J. Sen Lee, 1981*), (*J. Sen Lee et al., 2009*)

$$DN_{out} = [Mean] + K[DN_{in} - Mean] \tag{3}$$

Where *Mean = average of pixels in a moving window*

$$K = \frac{Var(x)}{[Mean]^2 \sigma^2 + Var(x)} \tag{4}$$

And

$$Var\,(x) = \left(\frac{[Variance\ within\ window] + [Mean\ within\ window]^2}{[\text{Sigma}]^2 + 1} \right) - [Mean\ within\ window]^2 \tag{5}$$

The Sigma filter uses Gaussian distribution probabilities, assuming that 95.5% of samples are within 2 standard deviations. To suppress noise, it replaces the pixel of interest with the average of DN values within the moving kernel that fall within this range (*J.-S. Lee, 1983*).

Median

The median filter is a simple method for removing pulse or spike noise. It suppresses or eliminates pulse functions shorter than half the width of the moving kernel, while retaining step and ramp functions (*Mansourpour et al., 2006*).

Therefore, the main aim of this article is to evaluate the suitability of Synthetic Aperture Radar (SAR) data for vegetation variability mapping. Through comparison with ground reference data, the effectiveness of SAR imagery in capturing variations in vegetation characteristics will be assessed.

MATERIAL AND METHODS

The experimental data for this study were obtained from the field with maize (49°50’43.3”N 16°16’27.7”E) located nearby the village Osík u Litomyšle belonging to the Dolní Újezd agricultural cooperative (ZD Dolní Újezd).

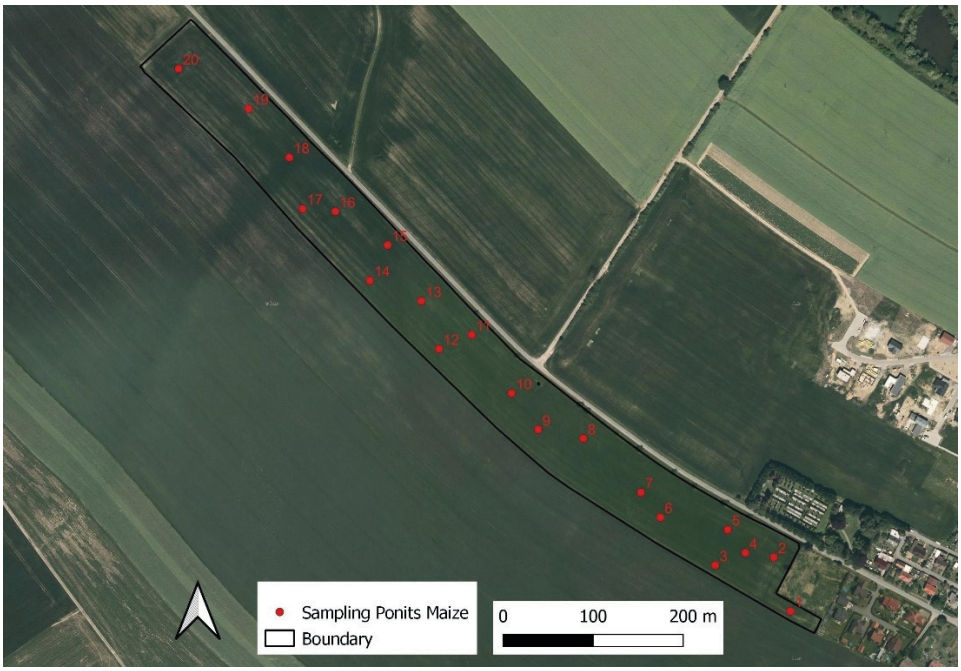

Fig. 1 Experimental field with sampling points
Obr. 1 Experimentální pole s odběrovými vzorky

Maize crops were sampled in an irregular network of twenty coordinated points (Fig. 1) arranged according to the production potential map. For our experiment, samples were taken and measured on July 3rd, 2023, when the corn was in the elongation growing stage. SAR data were downloaded from server dhr1.cesnet.cz (Collaborative Ground Segment - Czech Republic, n.d.). SAR imagery was obtained from the Sentinel-1 satellite mission operated by the European Space Agency (ESA). The satellite data covered by a temporal range corresponding to the study period. Ground reference data, including measurements of plant height, fresh weight, nitrogen content by NCrop chlorofylmetr (LeadingFarmers) and soil samples were collected using Mehlich-3 field techniques(Eckert & Watson, 1996). The acquired SAR data underwent preprocessing using the Sentinel Application Platform (SNAP) provided by ESA and Quantum Geographic Information System (QGIS) software. Cubic Convolution and Bilinear Interpolation resampling techniques were applied to the SAR imagery at pixel resolutions of 10, 50, and 100 meters.

Speckle filtering was conducted using Frost, Gamma Map, Lee Sigma, Median, Refined Lee, and Boxcar algorithms to mitigate noise and enhance data quality. Ter-

rain correction was performed using Range-Doppler Terrain Correction to account for topographic variations. The RVI index was computed using the formula (4sigmaVH)/(sigma*VV+sigmaVH), where sigma represents the backscatter coefficients for both horizontal (H) and vertical (V) polarization.

A statistical analysis was conducted to assess the correlation between SAR-derived metrics and ground reference data. Correlation coefficients and regression analyses were computed to evaluate the relationship between SAR imagery and field measurements. The accuracy of SAR-derived vegetation metrics was validated against ground reference measurements to assess the reliability and robustness of the methodology (*Yuan et al., 2018*), (*Nicolas et al., 2001*).

RESULTS

The correlation analysis examined the relationship between SAR-derived metrics and ground reference data. Different resampling techniques were assessed for their consistency with field measurements. Cubic Convolution combined with resampling to a 10-meter resolution consistently produced accurate results for fresh weight samples and plant height measurements, aligning well with ground reference data. Plant moisture content exhibited the weakest correlation with SAR data, indicating challenges in accurately estimating this parameter. Despite optimization attempts, no significant improvement in correlation was observed, highlighting the need for further research in this area.

Bilinear Interpolation emerged as the preferred technique for Ncrop measurements, outperforming other resampling methods in accurately estimating Ncrop levels from SAR imagery.

As can be seen from the correlation analysis between field measurements and speckle filtered SAR data in Tab. 1. Choosing multiple Speckle filters has given similar results across methods in green. However, differences were in the chosen method Bilinear Interpolation or Cubic Convolution.

In summary, selecting appropriate resampling techniques tailored to specific vegetation parameters is crucial. While Cubic Convolution and a 10-meter resolution were optimal for fresh weight samples and plant height, Bilinear Interpolation demonstrated superior performance for Ncrop measurements. These findings have implications for refining SAR data processing protocols to enhance vegetation variability mapping in agricultural contexts.

Table 1 Correlation analysis of SAR and field data – green indicates statistically important results
Tabulka 1 Korelační analýza ze SAR a naměřených dat – zelená indikuje statisticky významné výsledky

Field measurements	Speckl filters			
	Frost		Gamma_Map	
	Fros_10BI	Fros_10CC	GamM_10BI	GamM_10CC
Height	-0.510	-0.518	-0.510	-0.518
Fresh weight - whole plant	-0.640	-0.650	-0.640	-0.650
Plant moisture content	-0.088	-0.087	-0.088	-0.087
Ncrop	-0.616	-0.609	-0.616	-0.609
	IDANT		Lee_Sigma	
	IDAN_10BI	IDAN_10CC	LeeS_10BI	LeeS_10CC
Height	-0.510	-0.518	-0.510	-0.518
Fresh weight - whole plant	-0.640	-0.650	-0.640	-0.650
Plant moisture content	-0.088	-0.087	-0.088	-0.087
Ncrop	-0.616	-0.609	-0.616	-0.609
	Lee		Median	
	Lee_10BI	Lee_10CC	Medi_10BI	Medi_10CC
Height	-0.510	-0.518	-0.510	-0.518
Fresh weight - whole plant	-0.640	-0.650	-0.640	-0.650
Plant moisture content	-0.088	-0.087	-0.088	-0.087
Ncrop	-0.616	-0.609	-0.616	-0.609
	Refined_Lee		Boxcar	
	ReLe_10BI	ReLe_10CC	boxc_10BI	boxc_10CC
Height	-0.510	-0.518	-0.510	-0.518
Fresh weight - whole plant	-0.640	-0.650	-0.640	-0.650
Plant moisture content	-0.088	-0.087	-0.088	-0.087
Ncrop	-0.616	-0.609	-0.616	-0.609
		BI	Bilinear_Interpolation	
		CC	Cubic_Convolution	

DISCUSSION

The research findings hold implications for agricultural practices, particularly in the context of field monitoring supplemented by reliable radar data, offering potential enhancements in decision-making processes throughout the vegetational year. While traditional approaches, exemplified by (Mandal et al., 2020), typically involve monitoring entire fields with favorable outcomes, recent studies, such as (Hernández et al., 2022), have explored variability monitoring at the field scale, yielding promising results. Long-distance monitoring utilizing field data presents an opportunity to discern strengths and weaknesses in satellite remote sensing methodologies. The study acknowledges limitations due to the absence of alternative remote sensing methods for cross-validation of satellite data. Future directions may involve employing unmanned aerial vehicles (UAVs) or resampling data to finer resolutions, such as 5 meters, for comprehensive testing against

field data. The significance of these findings lies in the advancement of decision-making processes through the integration of field data with remote sensing techniques. It agrees with our results that variability monitoring has promising results.

(*Zoungrana et al., 2024*) presents a method for regional-scale wheat monitoring using Sentinel1 SAR and Sentinel-2 optical data. By employing a machine learning random forest classification algorithm on the Google Earth Engine platform, the study found that combining SAR and optical data significantly improved classification accuracy, achieving an 82.36% accuracy rate with a kappa coefficient of 0.77. These findings suggest that integrating SAR and optical data is effective for mapping wheat areas, with potential applications in agricultural planning and policy.

The findings from (*Zoungrana et al., 2024*) suggest that combining SAR and optical satellite data can significantly improve the accuracy of crop area classification and monitoring. This approach could be effectively applied to maize monitoring as well. Maize, like wheat, benefits from precise mapping of growing areas and timely monitoring of crop conditions. The integration of SAR and optical data could enhance the ability to estimate maize growth, detect stress, and predict yields more accurately. The methodology outlined in (*Zoungrana et al., 2024*) could be adapted for maize by adjusting the specific parameters and features relevant to maize growth and condition. In our results we cannot confirm or disagree with the approach, further research will be done.

(*Xu et al., 2022*) explores the estimation of maize biomass components—total biomass, leaf biomass, and stem biomass—using Sentinel-1 SAR polarizations and texture features. The study employed multi-label k-nearest neighbor (MLKNN) and multi-output support vector regression (MSVR) models, finding that mean texture features from SAR data were more effective predictors of biomass components than polarizations alone. MLKNN provided the best predictive accuracy, particularly when using texture features from combined VV and VH polarizations.

The findings from (*Xu et al., 2022*) provide a concrete example of how remote sensing data, particularly SAR texture features, can be used effectively in biomass estimation, which is a critical component of crop monitoring. These insights build on the broader themes discussed by authors, where the integration of advanced remote sensing techniques with field data is emphasized as a means to improve agricultural monitoring and decision-making. Together, these approaches underscore the growing importance of remote sensing in agriculture and the need for continued research into specific applications and methodologies, such as those explored in (*Xu et al., 2022*), to enhance the precision and utility of crop monitoring systems.

In our research we cannot agree or disagree with the findings presented. This approach will be in the future researched.

CONCLUSION

This study examined the integration of Synthetic Aperture Radar (SAR) imagery with ground reference data for maize cultivation, focusing on the preprocessing and resampling techniques utilized.

Cubic Convolution at a 10-meter resolution provided accurate estimates for fresh weight samples and plant height, showing a strong correlation with ground data. This

suggests that this resampling technique and resolution are well-suited for these specific agricultural parameters. On the other hand, Bilinear Interpolation was identified as the most effective method for accurately estimating Ncrop measurements, performing better than the other resampling techniques tested.

Despite these positive results, the study also highlighted the ongoing challenge of estimating plant moisture content using SAR data, which remains a complex and unresolved issue. We did a thorough evaluation of resampling techniques and the demonstration of the importance of selecting methods tailored to specific vegetation parameters for improving the accuracy of SAR-based agricultural monitoring. This research provides valuable insights for refining SAR data processing protocols, particularly in the context of vegetation variability mapping in agricultural environments.

Future research should focus on addressing the identified challenges, particularly the accurate estimation of plant moisture content. Further development and refinement of methodologies will be important for enhancing the reliability and precision of SAR imagery in monitoring vegetation health and variability, contributing to more informed agricultural practices.

ACKNOWLEDGMENT

We would like to thank the management of the ZD Dolní Újezd agriculture cooperative for providing agronomic data. This research was supported by the project of Ministry of Agriculture NAZV QK22010014.

REFERENCES

13. ZEMĚDĚLSTVÍ | ČSÚ. (n.d.). Retrieved May 10, 2024, from https://www.czso.cz/csu/czso/13-zemedelstvi-9012gu8xaa

Collaborative Ground Segment - Czech Republic. (n.d.). Retrieved May 10, 2024, from https://dhr1.cesnet.cz/#/home

ECKERT, D. J., WATSON, M. E. 1996. Integrating the Mehlich-3 extractant into existing soil test interpretation schemes. *Communications in Soil Science and Plant Analysis*, *27*(5–8), 1237–1249. https://doi.org/10.1080/00103629609369629

FROST, V. S., STILES, J. A., SHANMUGAN, K. S., HOLTZMAN, J. C. 1982. A Model for Radar Images and Its Application to Adaptive Digital Filtering of Multiplicative Noise. *IEEE Transactions on Pattern Analysis and Machine Intelligence*, *PAMI-4*(2), 157–166. https://doi.org/10.1109/TPAMI.1982.4767223

GitHub - GeomaticsAndRS/sar: Despeckling Synthetic Aperture Radar Images using a Deep Residual CNN. (n.d.). Retrieved September 3, 2024, from https://github.com/GeomaticsAndRS/sar

HERNÁNDEZ, M., BORGES, A. A., FRANCISCO-BETHENCOURT, D. 2022. Mapping stressed wheat plants by soil aluminum effect using C-band SAR images: implications for plant growth and grain quality. *Precision Agriculture*, *23*(3), 1072–1092. https://doi.org/10.1007/s11119-022-09875-6

IMPORTANCE OF MAIZE CROPPING-Web of Science Core Collection. (n.d.). Retrieved August 29, 2024, from https://www-webofscience-com.infozdroje.czu.cz/wos/woscc/full-record/WOS:000422176100013

KHABBAZAN, S., VERMUNT, P., STEELE-DUNNE, S., ARNTZ, L. R., MARINETTI, C., VAN DER VALK, D., IANNINI, L., MOLIJN, R., WESTERDIJK, K., VAN DER SANDE, C. 2019.

Crop monitoring using Sentinel-1 data: A case study from The Netherlands. *Remote Sensing*, *11*(16). https://doi.org/10.3390/RS11161887
KULKARNI, S. C., REGE, P. P. 2020. Pixel level fusion techniques for SAR and optical images: A review. *Information Fusion*, *59*, 13–29. https://doi.org/10.1016/j.inffus.2020.01.003
LEE, J.-S. 1983. NOTE Digital Image Smoothing and the Sigma Filter. *COMPUTER VISION, GRAPHICS, AND IMAGE PROCESSING*, *24*, 255–269.
LEE, J. Sen. 1981. Refined filtering of image noise using local statistics. *Computer Graphics and Image Processing*, *15*(4), 380–389. https://doi.org/10.1016/S0146-664X(81)80018-4
LEE, J. SEN, WEN, J. H., AINSWORTH, T. L., CHEN, K. S., CHEN, A. J. 2009. Improved sigma filter for speckle filtering of SAR imagery. *IEEE Transactions on Geoscience and Remote Sensing*, *47*(1), 202–213. https://doi.org/10.1109/TGRS.2008.2002881
LOPES, A., TOUZI, R., NEZRY, E. 1990. Adaptive Speckle Filters and Scene Heterogeneity. *IEEE Transactions on Geoscience and Remote Sensing*, *28*(6), 992–1000. https://doi.org/10.1109/36.62623
MANDAL, D., KUMAR, V., RATHA, D., DEY, S., BHATTACHARYA, A., LOPEZ-SANCHEZ, J. M., MCNAIRN, H., RAO, Y. S. 2020. Dual polarimetric radar vegetation index for crop growth monitoring using sentinel-1 SAR data. *Remote Sensing of Environment*, *247*, 111954. https://doi.org/10.1016/J.RSE.2020.111954
MANSOURPOUR, M., RAJABI, M. A., BLAIS, J. A. R. 2006. *EFFECTS AND PERFORMANCE OF SPECKLE NOISE REDUCTION FILTERS ON ACTIVE RADAR AND SAR IMAGES*.
NICOLAS, J. M., TUPIN, F., MAÎTRE, H. 2001. Smoothing speckled SAR images by using maximum homogeneous region filters: An improved approach. *International Geoscience and Remote Sensing Symposium (IGARSS)*, *3*, 1503–1505. https://doi.org/10.1109/IGARSS.2001.976892
OLIVER, C. J. 1991. Information from SAR images. *Journal of Physics D: Applied Physics*, *24*(9), 1493. https://doi.org/10.1088/0022-3727/24/9/001
THE INFLUENCE OF THE YIELD OF THE MAIZE HARVEST ON THE PROFITABILITY OF FARMS-Web of Science Core Collection. (n.d.). Retrieved August 29, 2024, from https://www-webofscience-com.infozdroje.czu.cz/wos/woscc/full-record/WOS:001121342700029
Understanding Synthetic Aperture Radar Images - Chris Oliver, Shaun Quegan - Knihy Google. (n.d.). Retrieved November 24, 2023, from https://books.google.cz/books?hl=cs&lr=&id=IeGKe40S77AC&oi=fnd&pg=PR17&ots=3fBXka4q9C&sig=WpouPQh_UDMyR82dDWlc4h7M-Xc&redir_esc=y#v=onepage&q&f=false
XU, C., DING, Y., & DAI, Z. (2022). Estimation of Maize Biomass Components from Sentinel-1 SAR Data Using Multi-Target Regressors. *International Geoscience and Remote Sensing Symposium (IGARSS)*, *2022-July*, 1392–1395. https://doi.org/10.1109/IGARSS46834.2022.9884054
YUAN, J., LV, X., & LI, R. (2018). A Speckle Filtering Method Based on Hypothesis Testing for Time-Series SAR Images. *Remote Sensing 2018, Vol. 10, Page 1383*, *10*(9), 1383. https://doi.org/10.3390/RS10091383
ZOUNGRANA, L. E., BARBOUCHI, M., TOUKABRI, W., BABASY, M. O., KHATRA, N. BEN, ANNABI, M., & BAHRI, H. (2024). Sentinel SAR-optical fusion for improving in-season wheat crop mapping at a large scale using machine learning and the Google Earth engine platform. *Applied Geomatics*, *16*(1), 147–160. https://doi.org/10.1007/S12518-023-00545-4

Corresponding author:
Miloš Láznička, +420607118401, laznickam@tf.czu.cz